

Mercury records covering the past 90 kyr from lakes Prespa and Ohrid, SE Europe

Alice R. Paine^{1*}, Isabel M. Fendley¹, Joost Frieling¹, Tamsin A. Mather¹, Jack H. Lacey², Bernd Wagner³, Stuart A. Robinson¹, David M. Pyle¹, Alexander Francke⁴, Theodore R Them II⁵, Konstantinos Panagiotopoulos³

¹Department of Earth Sciences, University of Oxford, Oxford, UK, OX1 3AN

²National Environmental Isotope Facility, British Geological Survey, Nottingham, UK

³Institute of Geology and Mineralogy, University of Cologne, Cologne, Germany

⁴Discipline of Archaeology, College of Humanities, Arts and Social Sciences, Flinders University, Adelaide, 5001, Australia

⁵Department of Geology and Environmental Geosciences, College of Charleston, Charleston, SC 29424, USA

*Corresponding Author: alice.paine@earth.ox.ac.uk

ABSTRACT

The element mercury (Hg) is a key pollutant, and much insight has been gained by studying the present-day Hg cycle. However, many important processes within this cycle operate on timescales responsive to centennial to millennial-scale environmental variability, highlighting the importance of also investigating the longer-term Hg records in sedimentary archives. To this end, we here explore the timing, magnitude, and expression of Hg signals retained in sediments over the past ~90 ka from two lakes, linked by a subterranean karst system: Lake Prespa (Greece/North Macedonia/Albania) and Lake Ohrid (North Macedonia/Albania). Results suggest that Hg fluctuations are largely independent of variability in common host phases in each lake, and the recorded sedimentary Hg signals show distinct differences first during the late Pleistocene (Marine Isotope Stages 2 – 5). The Hg signals in Lake Prespa sediments highlights an abrupt, short-lived, peak in Hg accumulation coinciding with local deglaciation. In contrast, Lake Ohrid shows a broader interval with enhanced Hg accumulation, and, superimposed, a series of low-amplitude oscillations in Hg concentration peaking during the Last Glacial Maximum, that may result from elevated clastic inputs. Divergent Hg signals are also recorded during the early and middle Holocene (Marine Isotope Stage 1). Here, Lake Prespa sediments show a series of large Hg peaks; while Lake Ohrid sediments show a progression to lower Hg values. Around 3 ka, anthropogenic influences overwhelm local fluxes in both lakes. The lack of coherence in Hg accumulation between the two lakes suggests that, in the absence of an exceptional perturbation, local differences in sediment composition, lake structure, Hg sources, and water balance all influence the local Hg cycle, and determine the extent to which Hg signals reflect local or global-scale environmental changes.

1. Introduction

Mercury (Hg) is a volatile metal released into the environment from both natural and anthropogenic sources, and actively cycled between surface reservoirs (e.g., atmosphere, ocean, lakes). Emissions

37 of Hg by geological processes are unevenly distributed across the Earth's surface, and are generally
38 concentrated where tectonic, volcanic, and geothermal activities are most intense (Rytuba, 2003;
39 Edwards et al., 2021; Schlüter, 2000). Geological processes have been major drivers of variability in
40 the global Hg cycle throughout Earth's history (Selin, 2009), leading to the use of sedimentary Hg to
41 reconstruct periods of intense volcanism (e.g., large igneous provinces (LIPs)) in Earth's geological
42 past (e.g., Grasby et al., 2019; Percival et al., 2018). In recent times, Hg release associated with
43 industrialisation, the extraction and combustion of fossil fuels, and natural resources (metals) has
44 overwhelmed the natural background flux (Outridge et al., 2018; Streets et al., 2019; United Nations
45 Environment Programme, 2018).

46 Existing in the atmosphere primarily in the form of gaseous elemental mercury, Hg has an
47 atmospheric lifetime of up to 2 years, facilitating its deposition far from the original source (Lyman et
48 al., 2020). Once removed from the atmosphere, Hg may enter vegetation and soils where it is cycled
49 between reservoirs by a complex series of processes, many of which occur on timescales that exceed
50 present-day monitoring (**Fig. 1**) (Branfireun et al., 2020; Selin, 2009). Evasion back to the
51 atmosphere, consumption by living organisms, or sequestration within aquatic sediments all represent
52 ways in which Hg may 'leave' the terrestrial environment, and aquatic sediments are known to be
53 particularly effective sinks within the global Hg cycle (Bishop et al., 2020; Selin, 2009). Here, microbial
54 processes lead to the formation of methylmercury (MeHg), which is the most bio-accumulative Hg
55 species and can cause severe neurological and physiological damage to complex organisms if
56 ingested (Driscoll et al., 2013; Wang et al., 2019).

57 The ecological and societal risks of environmental Hg contamination underscore the importance of
58 quantifying how natural and anthropogenic processes may influence Hg sequestration within aquatic
59 systems, and the timescales upon which they are effective. Time-resolved sediment records sourced
60 from marine and lacustrine basins are highly suitable for assessing these roles further back in time, as
61 the Hg deposited may originate from one of several potential sources in the atmospheric (e.g.,
62 precipitation, dust), terrestrial (e.g., soils, detrital matter), aquatic, and/or lithospheric domain (**Fig. 1**).
63 Thus, they can provide time-resolved records of Hg deposition, cycling, burial, and accumulation
64 relative to changing environmental conditions on a local, regional, or even global-scale (Cooke et al.,
65 2020; Zaferani and Biester, 2021), and so can offer new insights into the cycling of Hg in the
66 terrestrial realm.

67 Analysis of pre-industrial marine and lacustrine sediment records suggest that Hg concentration
68 broadly reflects variability in climate (Li et al., 2020). On orbital ($>10^3$ -year) timescales, oceanic Hg
69 signals manifest as low-amplitude fluctuations corresponding to global-scale climate shifts from warm
70 (interglacial) to colder (glacial) conditions; for example due to changes in atmospheric composition
71 (e.g., mineral dust loading) and circulation, biogeochemical cycling (Figueiredo et al., 2022), and/or
72 ocean circulation (Figueiredo et al., 2020; Gelety et al., 2007; Jitaru et al., 2009; Kita et al., 2016). On
73 centennial to millennial (10^2 - 10^3 -years) timescales, lacustrine Hg signals correspond more closely to
74 transient changes in hydrology, landscape dynamics, and ice/permafrost extent on local/regional
75 scales (Chede et al., 2022; Cordeiro et al., 2011; de Lacerda et al., 2017; Fadina et al., 2019; Li et al.,

76 2023; Pérez-Rodríguez et al., 2018, 2015) (**Fig. 1**). Importantly, climate-associated Hg signals
77 retained in lacustrine records integrate a range of processes and some records show higher
78 sedimentary Hg concentrations during cold, arid conditions (e.g., Li et al., 2020), while other records
79 tend to have higher Hg concentrations with warm and wet climates. For example, increases in
80 catchment-sourced detrital input have been proposed as the primary cause of Hg enrichment in
81 temperate lakes (Pan et al., 2020; Schütze et al., 2018), and near-shore marine records (Fadina et
82 al., 2019). Conversely, lakes located in glaciated regions may show dilution of Hg by the same inputs
83 (Schneider et al., 2020). Local, site-specific factors are therefore likely to influence sedimentary Hg
84 records. Yet, the combined effects of global and local processes complicate study of how changes in
85 the terrestrial Hg cycle may translate to measurable sedimentary signals and signals that are
86 comparable between different regional or global archives.

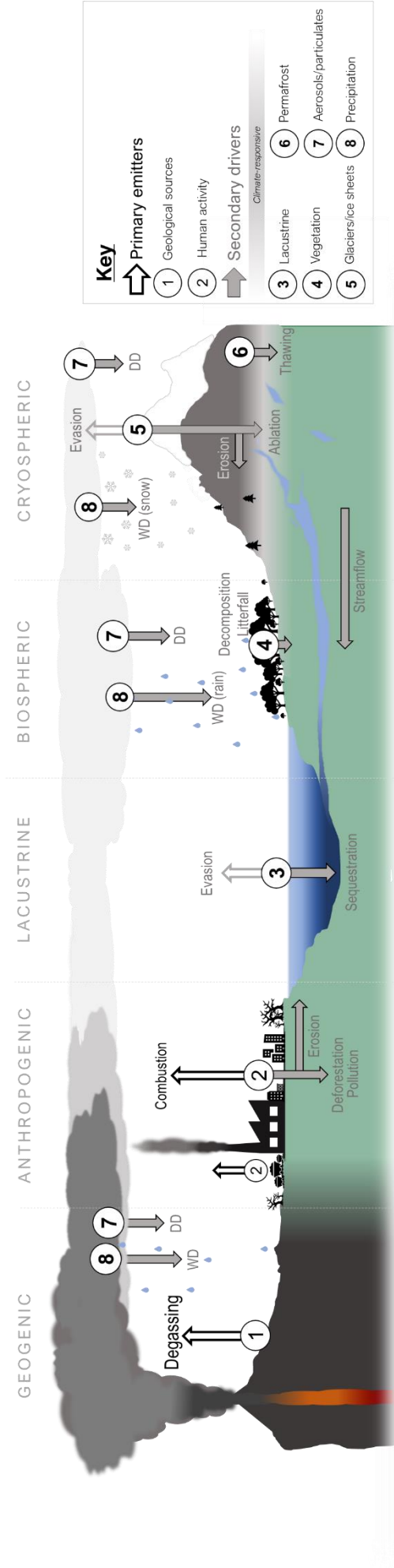


Figure 1: A summary diagram depicting the key anthropogenic, geogenic, biospheric, cryospheric, and lacustrine processes, which could generate and modify a sedimentary Hg signal over 10¹-10⁵-year timescales. Processes are abbreviated as: WD – wet deposition, DD – dry deposition. Non-filled arrows depict processes acting to increase the atmospheric Hg burden, and colour filled arrows depict processes acting to influence the quantity of Hg stored in terrestrial reservoirs. This figure is schematic (not drawn to scale), and constructed on the basis of reviews by Bishop et al. (2020), Obrist et al. (2018), Selin et al. (2009).

88 Sedimentary Hg presence (or absence) at discrete intervals can be quantified using the total Hg
89 concentration (Hg_T) (Bishop et al., 2020; Kohler et al., 2022; Nasr et al., 2011). However, internal
90 changes in bioproductivity, organic matter type and/or flux, sedimentation rate, pH, and redox
91 conditions could all produce a distinct, local, transient, sedimentary Hg enrichment without a
92 meaningful change in the total amount of Hg present and/or mobile in the broader aquatic system. In
93 light of these complexities, it has become common practice to examine total Hg concentration (Hg_T)
94 alongside Hg concentration divided by (normalised to) the concentration of various chemical species.
95 Normalisation is often applied when it can be shown that the abundance of a carrier (or “host”) phase
96 directly impacts Hg content. Normalisation (e.g. Hg/total organic carbon (TOC), Hg/total sulphur (TS))
97 may, in those cases, then reveal broader changes in environmental Hg availability (Grasby et al.,
98 2019; Percival et al., 2015; Shen et al., 2020; Them et al., 2019). Such an approach is particularly
99 beneficial for studies typically spanning $>10^2$ -year timescales, where the goal is to isolate the effects
100 of catchment-scale depositional and/or transport processes on Hg signals recorded in the sediment
101 through time.

102 Organic matter (hereafter represented by total organic carbon (TOC)) is generally considered the
103 dominant carrier phase of sedimentary Hg (Chakraborty et al., 2015; Ravichandran, 2004). For
104 records in which TOC and Hg co-vary linearly, Hg is generally normalized to TOC (Chede et al., 2022;
105 Figueiredo et al., 2022, 2020; Kita et al., 2016; Outridge et al., 2019). Some systems do not exhibit a
106 relation to TOC and Hg may instead be adsorbed onto (fine-grained) detrital minerals and detected by
107 a correlation between Hg and mineral-dominating elements such as aluminium (Al), titanium (Ti),
108 zirconium (Zr), rubidium (Rb), or potassium (K) (Sanei et al., 2012; Sial et al., 2013; Them et al.,
109 2019). In few cases, sulphide minerals may act as important Hg hosts (Benoit et al., 1999; Han et al.,
110 2008), however this is less common in freshwater lacustrine systems where sulphate-reduction is
111 often limited and only a small fraction of non-organic sulfur is buried (Ding et al., 2016; Holmer and
112 Storkholm, 2001; Tisserand et al., 2022; Watanabe et al., 2004).

113 Mercury’s relationship with other sedimentary components is often complex. For example, Hg_T may
114 also be suppressed through dilution by Hg-poor detrital or biogenic (carbonate, silica) material, and
115 Hg in many sediments is not exclusively or clearly modulated by balances between host-phase
116 abundance and dilution. Notably, this can also occur when the host-phases are always present in
117 sufficient quantities to sequester available Hg. In such cases, and where (single) host-phase
118 abundance or dilution cannot be easily accounted for, Hg accumulation rate (Hg_{AR}) may provide the
119 most optimal assessment of Hg availability through time as long as a robust age model is available for
120 the archive.

121 Sedimentary TOC, total sulphur (TS), and detrital and biogenic mineral concentrations change in
122 space and time, underscoring the need to assess how Hg covaries in relation to different host phases
123 and other sedimentary materials. Hydrology, sedimentation regime, and geochemistry may each
124 influence mercury host-phase availability and burial in a lacustrine system, and are likely to change
125 through time, highlighting the importance of investigating the longer-term records of Hg burial and
126 accumulation in sedimentary archives.

127 This study explores the timing, magnitude, and expression of Hg signals retained in the sediment
128 records of Lake Prespa (Greece/Albania/North Macedonia) and Lake Ohrid (North
129 Macedonia/Albania) over the past ~90 ka. The two lakes are located only ~10 km apart (**Fig. 2**), are
130 hydrologically connected by karst aquifers with ~50% of water inflow to Lake Ohrid originating from
131 Lake Prespa (Matzinger et al., 2006), and their sediments encode records of environmental change in
132 southeast Europe over the last ~90 ka (Damaschke et al., 2013; Francke et al., 2016; Leng et al.,
133 2010; Panagiotopoulos et al., 2014; Sadori et al., 2016; Wagner et al., 2010). Comparison of their
134 sedimentary records provides a rare opportunity to explore three important questions. First, we test
135 how the local sedimentary environment (e.g., host phase availability and sources) influences Hg
136 burial. Second, we investigate whether Hg signals reflect changes in catchment hydrology, structure,
137 and/or varying degrees of interaction between the two lake systems. Finally, we explore whether
138 regional-scale climate variability could have measurably affected the Hg signals retained in the
139 sediments.

140

141 **2. Site Description**

142 **2.1. Regional Climate**

143 The Mediterranean Sea and the European continent are both major influences on present-day climate
144 of the region surrounding lakes Prespa and Ohrid. Summer months (July to August) are hot and dry
145 (average monthly air temperature +26 °C) while winter months (November to January) are cold,
146 cloudy and wet, with an average monthly air temperature of –1 °C (Matzinger et al., 2006). Annual
147 precipitation in the region averages ~750 mm yr⁻¹, with winter precipitation falling predominantly as
148 snow at high elevations (Hollis and Stevenson, 1997). Present-day vegetation in the Prespa/Ohrid
149 region comprises a mixture of Balkan endemic, central European, and Mediterranean species
150 (Donders et al., 2021; Panagiotopoulos et al., 2014, 2020; Sadori et al., 2016).

151 Major shifts in sedimentation and catchment structure of lakes Prespa and Ohrid generally
152 correspond to the large-scale climate oscillations captured by proxy records across southern Europe
153 throughout the last glacial-interglacial cycle (~100-kyr) (e.g., Rasmussen et al., 2014; Sanchez Goñi
154 and Harrison, 2010; Tzedakis et al., 2006). Generally higher local temperatures and moisture
155 availability are observed during the last interglacial (pre-74 ka), following which conditions became
156 distinctly colder and/or drier. This resulted in the rapid recession of forest ecosystems, intense erosion
157 of local soils and catchments, and elevated aeolian activity (e.g., Panagiotopoulos et al., 2014; Sadori
158 et al., 2016; Francke et al., 2016). Although slightly warmer conditions were restored between ~57
159 and 29 ka, both moisture availability and temperature dropped again during the Last Glacial Maximum
160 (LGM; ~29 – 12 ka) – favouring the growth and development of glaciers and (peri)glacial features
161 (e.g., moraines) in the Prespa/Ohrid catchment (Ribolini et al., 2018; Gromig et al., 2018; Ruskiczay-
162 Rüdiger et al., 2020), but also across the Balkan peninsula (Allard et al., 2021; Hughes and
163 Woodward, 2017; Leontaritis et al., 2020). Lake Prespa's sediments host evidence for millennial scale
164 climate variability during the Last Glacial, which were tentatively correlated to Heinrich Events in the

165 North Atlantic (Wagner et al., 2010). At ~12 ka, the Pleistocene to Holocene transition saw the rapid
166 propagation of warmer, wetter conditions across the region (known as Termination I) with only brief
167 excursions from this warming trend, such as episodes of transient drying and/or cooling at 8.2 ka and
168 4.2 ka (Bini et al., 2019; Aufgebauer et al., 2012a). Anthropogenic influence on the Balkan landscape
169 becomes increasingly clear from ~2.5 ka onwards, mainly in the form of increased erosion regimes,
170 forest clearance, agricultural land modification, and evidence for metallurgic practices
171 (Panagiotopoulos et al., 2013; Cvetkoska et al., 2014; Radivojević and Roberts, 2021).

172

173 **2.2. Lake Prespa**

174 The Prespa lake system (40°54' N, 21°02' E) is composed of two lakes separated by an isthmus and
175 located on the tripoint of North Macedonia, Albania and Greece, at an altitude of 844 metres (m)
176 above sea level. The ~1300 km² catchment of the Prespa lakes encompasses the Pelister Mountains
177 to the east and the Galičica Mountains to the southwest and west (**Fig. 2**). Here we focus on Megali
178 Prespa (hereafter referred to as Lake Prespa), the larger of the two lakes, which has a surface area of
179 254 km², a maximum water depth of 48 m, and a mean water depth of 14 m. The total inflow into Lake
180 Prespa averages ~16.9 m³ s⁻¹ (Matzinger et al., 2006). Water input is sourced from surface runoff
181 (56%), direct precipitation (35%), and inflow from the smaller of the two lakes (Mikri Prespa; 9%)
182 (Matzinger et al., 2006). Lake Prespa has no surface outflow. The residence time of the lake's waters
183 is ~11 years (Matzinger et al., 2006) and water is predominantly lost through evaporation (52%),
184 underground karst channels into Lake Ohrid located 10 km to the west (46%), and irrigation (2%). The
185 lake is currently mesotrophic with an average total phosphorus (TP) concentration of 31 mg m⁻³ in the
186 water column, basal anoxia in summer months, and generally clear waters; all signalling moderate
187 biological productivity (Hollis and Stevenson, 1997). However, the lake likely held a more oligotrophic
188 (low) nutrient status during the colder late Pleistocene, where biological productivity reduced
189 substantially (Matzinger et al., 2006; Wagner et al., 2010).

190

191 **2.3. Lake Ohrid**

192 Lake Ohrid (41°02' N, 20°43' E) lies 693 m above sea level. Separated from Lake Prespa by the
193 Galičica Mountains, the lake straddles the boundary between North Macedonia and Albania (**Fig. 2**).
194 The lake is ~30 km long and 15 km wide, with a maximum water depth of 293 m, water volume of
195 55.4 km³, and hydraulic residence time of ~70 years. Water input is sourced from direct precipitation
196 (23%), river inflow (24%), and karst springs (53%) fed by precipitation and water from Lake Prespa
197 (Matzinger et al., 2006; Lacey and Jones, 2018), and this hydrological link increases the Ohrid
198 catchment by ~1300 km² to ~2610 km². Evaporation (40%) and outflow via the river Crn Drim (60%)
199 are the dominant pathways for water loss from Lake Ohrid, and complete mixing of the lake occurs
200 only every few years (Matzinger et al., 2006). The present-day lake shows low levels of biological

201 productivity (oligotrophic) with an average dissolved phosphorus content of 4.5 mg m^{-3} , and regular
 202 mixing maintains moderately oxygenated bottom waters (Matzinger et al., 2006; Wagner et al., 2010).

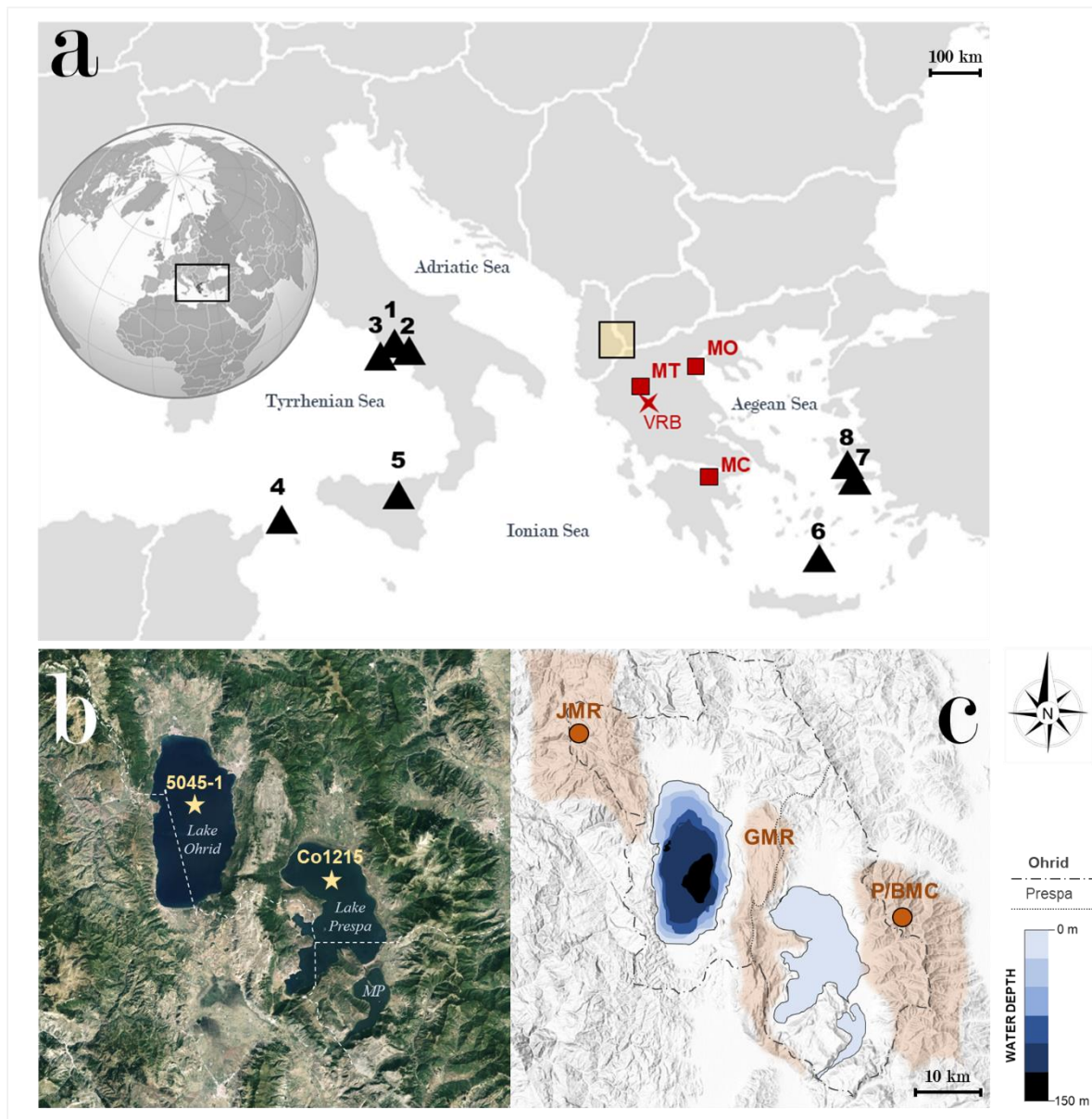


Figure 2: (a) Map showing the location of lakes Prespa and Ohrid within Southern Europe (yellow shaded box). Volcanoes from which tephra has been identified in Co1215 (Prespa) and/or 5045-1 (Ohrid) are coloured as black triangles, and numbered as: 1 – Vesuvius, 2 – Campi Flegrei, 3 – Ischia, 4 – Pantelleria, 5 – Etna. Volcanoes of the South Aegean Volcanic Arc with known explosive eruptions (>magnitude 4.0) between 90 and 0 ka are also numbered: 6 – Santorini, 7 – Nisyros, 8 – Yali. Sites referred to in this study are also labelled as follows: (red squares) MT – Mount Tymphi, MO – Mount Olympus, MC – Mount Chelmos; (red star) VRB – Voidomaitis river basin. (b) Aerial photo showing the coring locations of Co1215 and 5045-1, and illustrating the vegetation distributions of the area surrounding lakes Prespa and Ohrid. Mikri Prespa is labelled as ‘MP’ Base image sourced from GoogleEarth v 9.177.0.1™. (c) Hillshade map of the Prespa/Ohrid region and bathymetric data of lakes Prespa and Ohrid (Jovanovska et al., 2016; Wagner et al., 2022). Grey dashed lines denote watershed boundaries for lakes Prespa and Ohrid, respectively adapted from Panagiotopoulos et al. (2019). Basemap sourced from ArcGIS v 10.0™ (spatial reference 102100 (3857)). Orange shading denotes mountain ranges are labelled as: P/BMC – Pelister/Baba mountain chain (circle marking the location of Mount Pelister: 2601 m a.s.l.), GMR – Galičica mountain range, and JMR – Jablanica mountain range (circle marking the location of Jablanica Mountain - 2257 m a.s.l.). All mountain ranges contain evidence for the presence of glaciers and/or (peri)glacial features of late Pleistocene age (Hughes et al., 2022, 2023)

203 **3. Methods**

204 **3.1. Lake Prespa (Co1215)**

205 Composite core Co1215 was recovered in autumn 2009 and summer 2011 from the central-northern
206 section of Lake Prespa (40°57'50" N, 20°58'41" E, **Fig. 2**). Sediment recovery was performed using a
207 floating platform, with a gravity corer for surface sediments and a 3-m-long percussion piston corer
208 (UWITEC Co. Austria) for deeper sediments. Overlapping 3-m-long sediment cores were cut into
209 segments of up to 1 m in length for transport and storage. After splicing and correlation of core
210 segments according to geochemical and optical information, the resulting 17.7 m composite core was
211 continuously sampled at 2-cm-resolution, yielding a total of 849 samples. It is comprised of three
212 major lithofacies, which differ in colour, sediment structure, grain size, organic-matter and carbonate
213 content, and geochemistry. There are no lithological indications of any hiatuses or instances of non-
214 contiguous sedimentation in core Co1215. A detailed lithostratigraphic characterisation of the entire
215 succession (90–0 ka) is presented in Damaschke et al. (2013), along with details of the six visible
216 tephra layers and five cryptotephra layers identified in Co1215 (**Table S3**).

217 Published data for Lake Prespa (Co1215) includes: total carbon (TC), total inorganic carbon (TIC),
218 and total sulphur (TS) analyses (Aufgebauer et al., 2012; Damaschke et al., 2013). These data were
219 measured at ~2 cm resolution with a DIMATOC 200 (DIMATEC Co., Germany), and TS using a Vario
220 Micro Cube combustion CNS elemental analyser (VARI O Co.) at the University of Cologne. TOC was
221 calculated as the difference between TC and TIC by Aufgebauer et al. (2012) for the upper ~3.2 m,
222 and by Damaschke et al. (2013) for the full ~17 m succession. The inorganic chemistry of the
223 sediments was determined by X-ray fluorescence (XRF) data, generated using an ITRAX core
224 scanner (COX Ltd., Sweden) equipped with a Mo-tube set to 30 kV and 30 mA, and a Si-drift chamber
225 detector (Wagner et al., 2012). Core Co1215 was scanned with a resolution of 2 mm and a scanning
226 time of 10 seconds per measurement. Elemental intensities were obtained for potassium (K), titanium
227 (Ti), manganese (Mn), strontium (Sr), iron (Fe), calcium (Ca), and rubidium (Rb) (Wagner et al.,
228 2012).

229

230 **3.1.1. Chronology**

231 A chronology for Co1215 was previously produced by linear interpolation using volcanic ash layers,
232 coupled with ¹⁴C and electron spin resonance (ESR) dates obtained for bulk organic, fish, and aquatic
233 plant remains (Aufgebauer et al., 2012). Here, we update this chronology with a Bayesian age-depth
234 model that re-calculates previously obtained ¹⁴C-dates (**Table S4**) with the latest (Intcal2020)
235 radiocarbon calibration (**Fig. 3**) (Reimer et al., 2020). We used rBacon v 2.5.7 (Blaauw and Christen,
236 2011), and the new age model includes updated ⁴⁰Ar/³⁹Ar dates of two eruptions geochemically
237 correlated to specific tephra layers within the Prespa core (Damaschke et al., 2013); the Y-5 (39.85 ±
238 0.14 ka, 2σ (Giaccio et al., 2017)) and Y-6 (45.50 ± 1 ka, 2σ (Zanchetta et al., 2018; Scaillet et al.,
239 2013)) tephra units. Every tephra layer is assumed to have been deposited instantaneously. The final

240 model used herein presents the median of all the iterations (generally indistinguishable from the
 241 mean), and when referring to ages of specific depths within the core we include the 95% confidence
 242 intervals. The upper 2 m (Holocene) section of core Co1215 is chronologically well constrained by 10
 243 ¹⁴C dates and two tephra layers, with modelled age uncertainties in this section ranging from ~5 to
 244 580 years. Uncertainty increases with depth due to the lack of independent chronological anchors
 245 available. For example, three ESR dates for a shell fragment layer (~14.6 m depth) give an average
 246 age of 73.6 ± 7.7 ka, and form the only tie point currently available below 8.5 m. All twenty-seven tie-
 247 points and accompanying chronological details are presented in **Text S13** and **Table S3**. Our revised
 248 model shows broad agreement with the interpolation-based chronology presented by Damaschke et
 249 al. (2013), and suggests that core Co1215 provides a continuous record of sedimentation over the
 250 past ~90-kyr (**Fig. S1**), with each 2 cm sample equating to ~100 years (on average).

251

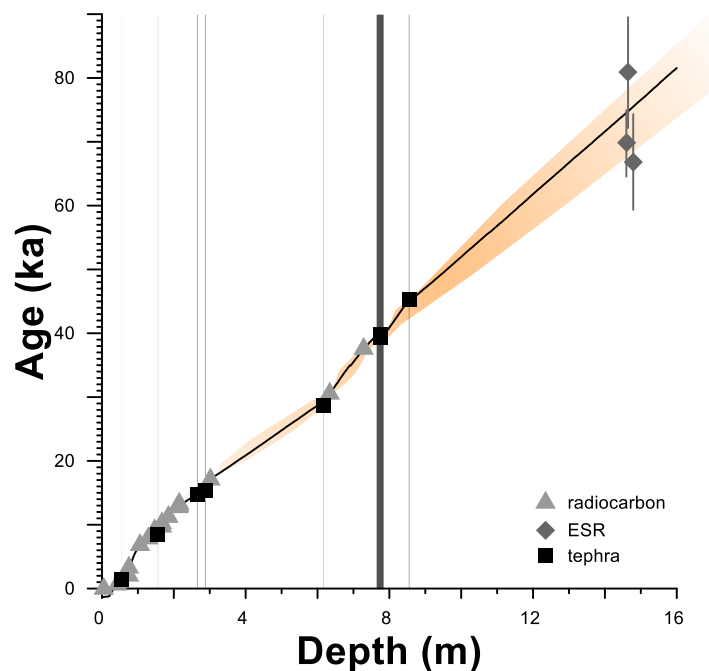


Figure 3: A Bayesian age-depth model for core Co1215 from Lake Prespa. Calibrated ages for the twenty-seven tie points used in model generation are displayed by type: radiocarbon-dated bulk organic, fish, or aquatic plant remains (light grey triangles), volcanic tephra layers (black squares) and electron-spin resonance (ESR)-derived dates for a shell layer (*Dreissena*) located at 14.63–14.58 m depth (dark grey diamonds). Uncertainties for ESR dates at 1 σ are presented as dark grey vertical lines. Black line marks the median core age predicted by the model, which is generally indistinguishable from the predicted mean. Minimum and maximum model ages at 95% (2 σ) confidence are marked with orange shading. Grey bars mark the stratigraphic placement of tephra layers used as tie-points, and widths of these bars are proportional to the thickness of the tephra layers within the core, respectively. Uncertainties for radiocarbon and tephra dates are within the displayed point sizes, and presented in **Table S4**.

252

253 3.2. Lake Ohrid (core 5045-1)

254 The 5045-1 coring site (“DEEP”) is located in the central part of Lake Ohrid (41°02’57” N, 20°42’54” E)
 255 (**Fig. 2**). The uppermost 1.5 m of sediments at DEEP were recovered in 2011 using a UWITEC
 256 gravity and piston corer. Sediments below 1.5 m depth were recovered from six closely-spaced drill
 257 holes at the site in 2013 (5045-1A to 5045-1F), with a total composite field recovery amounting to >

258 95% (545 m); accounting for overlap between cores (Wagner et al., 2014b). Sediment cores were
259 spliced to a composite record using optical and geochemical information. For sedimentological and
260 geochemical analyses, 2 cm thick slices (40.7 cm³) were removed from the core at a resolution of 16
261 cm (~480-yr) at the University of Cologne. For this study, we analysed 217 samples from between 0
262 and 36.27 m composite depth. We cannot entirely rule out that changes in sedimentation occurred
263 between samples, however, recent seismic (Lindhorst et al., 2015), borehole logging (Ulfers et al.,
264 2022) and sedimentological studies (Wagner et al., 2022, 2019) suggest that sedimentation at the
265 DEEP site has been near-continuous since ~1.3 Ma, with no clear evidence for any major (>1-kyr)
266 hiatuses. A detailed lithostratigraphic characterisation of the 5045-1 core succession is presented by
267 Francke et al. (2016). Details of the six microscopic and two visible tephra layers identified in the ~36
268 m section analysed in this study are presented by Leicher et al. (2021), and listed in **Table S5**.

269 The Hg data obtained from core 5045-1 (Lake Ohrid) are presented herein alongside two previously
270 existing datasets. The first dataset comprises TC and TIC measured using a DIMATOC 200 (TOC
271 calculated as the difference between TC and TIC), and TS using a Vario Micro Cube combustion CNS
272 elemental analyser at the University of Cologne - both by Francke et al. (2016). The second dataset
273 comprises XRF data obtained using an ITRAX XRF core scanner at the University of Cologne at 2.56
274 m increments, carried out on 2 cm thick samples, and processed using QSpec 6.5 software (Cox
275 Analytical) by Francke et al. (2016). Elemental intensities were obtained for K, Ti, Fe, Zr, and Ca. To
276 validate the quality of the XRF scanning data, conventional wavelength dispersive XRF (WDXRF,
277 Philips PW 2400, Panalytical Cor.) was conducted on the 2-cm-thick samples at 2.56-m resolution.
278 ITRAX data for each WDXRF sample was averaged to ensure comparability with the conventional
279 XRF data, and r^2 values were to compare ITRAX and WDXRX datasets (Francke et al. (2016).

280

281 **3.2.1. Chronology**

282 This study uses the age-depth model generated by Francke et al. (2016), and extended by Wagner et
283 al. (2019) for the upper ~248 m and ~447 m of core 5045-1, respectively. Both combined
284 tephrochronological data with orbital parameters using a Bayesian age modelling approach (Bacon
285 2.2). Tephra layers were used as first-order constraints. From the eleven total ³⁹Ar/⁴⁰Ar dated tephra
286 layers employed in Wagner et al. (2019), seven are found in the upper ~36 m section analysed in this
287 study. The age of the eighth tie-point (OH-DP-0009) is defined following geochemical correlation of
288 this tephra layer to the AD472/512 eruption of Somma-Vesuvius, Italy (Francke et al., 2019; Leicher et
289 al., 2021). This chronological information was coupled with climate-sensitive proxy data (TOC and
290 TIC) to define cross-correlation/inflection points with orbital parameters, which were included in the
291 age–depth model as second-order constraints (**Table S6**). Four of these points correspond to the ~36
292 m interval analysed in this study (Wagner et al., 2019). The 95% confidence intervals of ages for
293 specific depths produced by the model average at ±5.5 kyr, with a maximum of ±10.6 kyr. The
294 resulting chronology suggests that the 0.97-36.27 m core section analysed here covers the time
295 interval 1.6 – 89.6 ka, with each sample possessing a resolution of ~400 years (Francke et al., 2016;

296 Wagner et al., 2019). Full description of the 5045-1 chronology and associated methods are
297 presented in **Supplementary Text SI4**.

298

299 **3.3. Mercury measurements**

300 Total Hg concentrations (Hg_T) in the bulk sediments of cores 5045-1 (Ohrid) and Co1215 (Prespa)
301 were measured using an RA-915 Plus Portable Mercury Analyzer with PYRO-915 Pyrolyzer, Lumex
302 (Bin et al., 2001) at the University of Oxford. Samples were analysed for Hg_T at a resolution of ~2 cm
303 for Co1215 (Lake Prespa), and ~16 cm for 5045-1 (Lake Ohrid) (see sections **3.1** and **3.2**).

304 Approximately 2 cm³ of sediment was homogenized to fine powder for TOC (Wagner et al., 2019;
305 Francke et al., 2016; Aufgebauer et al., 2012a; Damaschke et al., 2013) and Hg analyses (this study).
306 For Hg analysis, powdered samples were weighed into glass measuring boats, with masses ranging
307 between 35–96 mg for Co1215, and between 27–78 mg for 5045-1. For samples particularly rich in
308 inorganic fractions (e.g., samples coinciding with tephra layers), masses needed to be greater in order
309 to yield a sufficiently high peak area (Lumex output) for calculation of sediment mercury
310 concentrations. Samples were then placed into the pyrolyzer (Mode 1) and heated to ~700°C,
311 volatilizing any Hg in the sample. Spectral analysis of the gases produced yields the total Hg content
312 of the sample. Six measures of standard material (paint-contaminated soil – NIST Standard
313 Reference Material ® 2587) with an expected Hg concentration of $290 \pm 9 \text{ ng g}^{-1}$ (95% confidence)
314 were run to calibrate the instrument prior to sample analysis, and then one standard between every
315 10 lacustrine samples (calibration results in **Supplementary Information**). Long-term observations of
316 standard measurements with total Hg yield similar to the sediment samples analysed here indicate
317 reproducibility is $\pm 6 \%$ or better for Hg concentrations $>10 \text{ ng g}^{-1}$ (Frieling et al., 2023), and with Hg
318 recovery close to 100% as expected from pyrolysis-based instrumentation (Bin et al., 2001). Details
319 of standard runs for each core are included as a supplementary file.

320

321 **3.3.1. Mercury accumulation**

322 Rates of Hg accumulation in both cores were calculated by:

$$323 \quad Hg_{AR} = Hg_T (DBD \times SR) \quad (eqn. 1)$$

324 where Hg_{AR} is the total Hg mass accumulation rate ($\text{mg m}^{-2} \text{ kyr}^{-1}$), Hg_T is the total mercury
325 concentration (expressed in mg g^{-1}), DBD is the dry bulk density (g m^{-3}), and SR is the sedimentation
326 rate (SR) in m kyr^{-1} . Values for Hg_{AR} are also calculated with respect to the median age estimate for
327 each sample, meaning that uncertainties increase with depth.

328 Sedimentation rates for both Prespa and Ohrid were calculated by combining stratigraphic and
329 lithological observations with the age-depth relationship ascertained for each core, respectively. For
330 Lake Prespa, we calculate the sedimentation rate using the updated age-depth model presented in
331 **section 3.1.2**. Dry bulk density values were calculated on the basis of sedimentological data available

332 for each core. For the Lake Ohrid dataset, DBD values were already available following the analyses
333 of Francke et al. (2016). To acquire these values for Lake Prespa, we employed the formula:

334
$$DBD = M_{solid} / V_{total} \quad (eqn. 2)$$

335 where M_{solid} is the mass of dry solid material (g) measured in each sample, and V_{total} is the volume of
336 each respective sample (2 cm³). Values for M_{solid} were calculated based on recorded weight loss
337 between wet and dry samples taken for CNS analyses by Aufgebauer et al. (2012), assuming an
338 average wet density of 1 g cm⁻³ for wet sediments, and 2.6 g cm⁻³ (grain density) for dry sediments.

339 For Lake Ohrid, we utilise the sedimentation rate values calculated by Wagner et al. (2019), and dry
340 bulk density measurements measured by Francke et al. (2016) (see these publications for full
341 methods).

342

343 **3.4. Mercury normalization**

344 The availability of specific host phases is often assumed to exert control on the sedimentary burial of
345 Hg. Here, we test if the Hg deposited into the sediments of lakes Prespa and Ohrid may be impacted
346 by abundance of a suite of phases. To do this, we assess both Hg_T records relative to quantitative
347 estimates of TOC and TS (assuming sulphides contribute to TS): both considered potential host
348 phases of Hg in sedimentary successions (Chakraborty et al., 2015; Garcia-Ordiales et al., 2018;
349 Ravichandran, 2004; Shen et al., 2020).

350 Detrital minerals constitute another potential host phase of Hg in sedimentary records. Elements such
351 as Al, Ti, K, Zr, and Rb are commonly used as proxies for this purpose (Kongchum et al., 2011;
352 Percival et al., 2018b; Shen et al., 2020). We observe a close correlation between K and Ti in Lake
353 Prespa, and quartz in Lake Ohrid (**Fig. S2**): all proxies for fine-grained material inputs to a lake basin
354 (Grygar et al., 2019; Warrier et al., 2016). To facilitate direct comparison of the two cores, we assess
355 the relative abundances of (fine-grained) detrital material using XRF-based K counts. To account for
356 differences in resolution between Hg and XRF data, K measurements were averaged to the thickness
357 of each discrete Hg sample, and K values corresponding to the Hg sample depths extracted.

358 In line with previous studies (Shen et al., 2020), we assume that the strongest positive-sloped linear
359 correlation with Hg among the analysed elements TS, TOC, and K signals the most likely dominant
360 influence on Hg loading in each core, which may then be interpreted as the 'host-phase'. However, it
361 is conceivable that different host phases may dominate in different sections of the individual cores or
362 that no single host-phase clearly dominates, and so the same approach is also applied restricted to
363 the data within each individual marine isotope stage (MIS) (**Table 1**).

364

365

366 4. Results & Discussion

367 Sediment cores extracted from Lake Prespa (Co1215) and Lake Ohrid (5045-1) provide a detailed,
368 time-resolved record of Hg cycling between ~90 and 0 ka. Results are presented with direct reference
369 to key stratigraphic intervals: the Holocene (12–0 ka; MIS 1), and the late Pleistocene (120 –12 ka;
370 MIS 2–5). Widespread proxy-based evidence for warmer temperatures, forest expansion, and
371 increased precipitation representative of interglacial climatic conditions marks the start of the
372 Holocene epoch (~12 ka) in SE Europe (Kern et al., 2022; Panagiotopoulos et al., 2014; Sadori et al.,
373 2016; Tzedakis et al., 2006). For simplicity, we hereafter equate “MIS 1” to the Holocene, allowing a
374 clearer distinction between glacial (late Pleistocene) and interglacial (Holocene) climate conditions.
375 We use these time-slices, that also represent broad climate and environmental ‘modes’, as a
376 framework upon which the Hg composition of both cores can be directly compared relative to local
377 changes in sediment lithology and geochemistry (**Table 1**), and a foundation upon which local and
378 regional-scale environmental changes can be assessed relative to global shifts in glaciation, climate,
379 sea level, and ocean circulation. We first consider the extent to which soft sediment processes
380 (**section 4.1**) and lithological features (**section 4.2.**) may have influenced the Hg variability observed
381 in **Figures 5** and **6**, before adopting a catchment-scale perspective in **section 4.3** to explore the role
382 of diverse environmental processes in Hg cycling through these two systems.

383 **Table 1:** A comparison of the features of cores Co1215 (Lake Prespa) and 5045-1 (Lake Ohrid) relative to the late Pleistocene
 384 (LP; 120 – 12 ka), the Holocene (H; 12 – 0 ka), and the marine isotope stage (MIS) stratigraphic framework defined in Lisiecki
 385 & Raymo (2005)*. Hg_T is given in ng g⁻¹, and Hg_{AR} is given in mg m⁻² kyr⁻¹.

			Depth (m)	Mean		Sedimentology**	
				Hg _T	Hg _{AR}	Lithology	Key Features
Lake Prespa	Holocene	MIS 1	2.4–0	64.6	11.9	Silt gyttja. Decreasing sand content with depth.	High lake levels. One visible and one microscopic tephra layer. High microcharcoal and green algae concentrations. High TOC/TN ratios. High sedimentation rate.
	Late Pleistocene	MIS 2	6–2.4	41.9	12.6	2.9–2.4 m – High fine sand (<250 µm), with clayey silt and evidence of lamination.	Increasing lake level. Two cryptotephra layers. Transient nutrient pulse 12.8–11.7 ka. Moderate TOC and low TIC.
						6–2.9 m – Homogenous sediment structure. Silt, distinct lamination and siderite precipitation.	Evidence for ice-rafted debris deposition. Low productivity and lake level. High K and organic δ ¹³ C. Low water δ ¹⁸ O. Declining C/N ratios. High sedimentation rate.
		MIS 3	11–6.1	32.8	7.2	6.6–6.1 m – Massive sediment structure. Silt with distinct lamination.	Steady decrease in lake level. High oxygen index.
						11–6.6 m – Massive sediment structure. Silt.	Increasing lake level. Four visible and three microscopic tephra layers. High C/N ratios. Moderate TOC, very low TIC.
	MIS 4	13.9–11	33.7	9.4	Massive sediment structure. Clayey silt.	High sedimentation rate. Very low TOC. No tephra layers. Low productivity. Declining C/N ratios. High K content gives evidence for ice-rafted debris deposition.	
MIS 5a-c	17.7–13.9	44.2	10.0	15.2–13.9 m – Massive, bioturbated sediments. Clayey silt and fine sand.	Increasing lake level and high productivity. <i>Dreissena</i> shell layer 14.58–14.56 m.		
				17.8–15.2 m – Massive sediment structure. Clayey silt with fine sand (a).	Deep lake with moderate/low productivity High green algae concentrations. High TOC, low TIC.		
Lake Ohrid	Holocene	MIS 1	4.6 – 1.1	47.2	26.2	3–0 m – Massive sediment structure. Bright colouring indicates high calcite; dark colouring indicates lower calcite.	High productivity. Four microscopic tephra layers. Low K concentrations. High sedimentation rate.
						4.6–3 m – Slightly calcareous silty clay and massive sediment structure. Frequent siderite-rich layers.	Low TIC and calcite. High iron availability. Low productivity and stronger calcite dissolution. High K concentrations. High sedimentation rate.
	Late Pleistocene	MIS 2	11.3 – 4.6	69.2	45.5	Silty clay. Mottled, often massive sediment structure. Frequent siderite-rich layers. Abundant fine fraction (< 4 µm) sediments.	Very low TIC, TOC, and calcite suggesting low productivity, with large inputs of fine-grained, and chemically weathered siliciclastics. High iron availability. Two visible and two microscopic tephra layers. Mass-movement deposit at 7.87 m.
		MIS 3	23–11.3	50.6	33.4		
		MIS 4	28.8–23	50.2	29.6		
		MIS 5a-c	36.3–28.8	36	20.4	35.6 – 28.8 m – Silty clay with a massive sediment structure. Bright colouring indicates high calcite; dark colouring indicates lower calcite.	Low siliciclastic mineral abundance. Decreasing δ ¹⁸ O and δ ¹³ C. Strong primary productivity. Low sedimentation rate.
36.6 – 35.6 m – Silty clay. Mottled, often massive sediment structure. Frequent siderite-rich layers.	Higher carbonate δ ¹⁸ O and δ ¹³ C corresponds to reduced TIC, and high siderite. Low sedimentation rate.						

386
 387 * MIS 5a-c – 96–71 ka; MIS 4 – 71–57 ka; MIS 3 – 57–29 ka; MIS 2 – 29–12 ka; MIS 1 – 12–0 ka.
 388 **Summarised from the following references:

389 Lake Prespa - (Aufgebauer et al., 2012; Cvetkoska et al., 2015; Damaschke et al., 2013; Leng et al., 2013; Panagiotopoulos et al., 2014; Wagner
 390 et al., 2014)
 391 Lake Ohrid - (Francke et al., 2016, 2019; Just et al., 2015; Lacey et al., 2016; Leicher et al., 2021; Wagner et al., 2019)
 392

393 4.1. Host Phase Controls

394 The availability and abundance of specific host phases is often assumed to control sedimentary Hg
 395 accumulation and burial (Outridge et al., 2007). Both Lake Prespa and Lake Ohrid show evidence for
 396 complex relationships between Hg_T, TOC, TS, and K concentrations through time (Fig. 4). However,
 397 the trends displayed in Figure 4 also suggest that: (1) the strength of the relationships between Hg,
 398 TOC, TS, and detrital minerals (K) are distinctly different between the two lakes, and (2) the Hg_T
 399 signals preserved in Lake Prespa and Lake Ohrid cannot be fully explained by variability in
 400 abundance of these potential host phases individually.

401

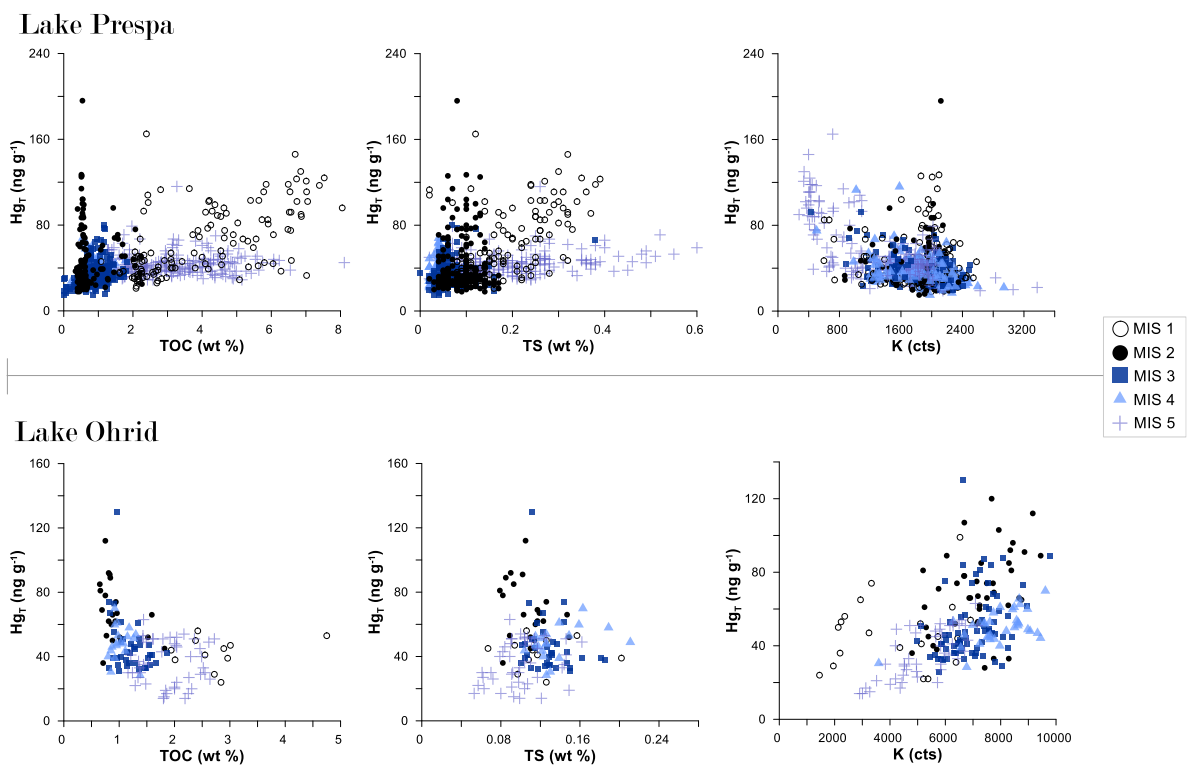


Figure 4: A comparison of host-phase relationships between lakes Prespa and Ohrid. Points are coded relative to stratigraphic period: the Holocene (12–0 ka, transparent circles), and the late Pleistocene (90–12 ka, filled symbols). We compare Hg_T records for both lakes relative to total organic carbon (TOC), sulphide (estimated by total sulphur (TS)), and detrital minerals (estimated by potassium (K) concentrations) – note that aluminium (Al) data are more commonly used as an indicator of detrital mineral abundance but these are currently unavailable for 5045-1.

402

403 Core Co1215 from Lake Prespa shows a moderate correlation between Hg_T and TOC during the
 404 Holocene and late Pleistocene (all data in Fig. 4; Table 1). This correlation is most significant during
 405 the Holocene (MIS 1), where distinct enrichments in Hg_T occur in conjunction with a similarly sharp

406 increase in TOC, and low variability in Hg/TOC values (**Fig. 5**). However, it is more inconsistent during
407 the late Pleistocene (MIS 2–5). For example, the highest Hg_T values are measured in the relatively
408 TOC-lean sediments of MIS 2 (**Fig. 4, 5**), and a plateau also appears when higher TOC
409 concentrations are reached during MIS 5 whereby Hg_T no longer increased in step with TOC (**Fig. 4,**
410 **S2**). The correlations observed are not strong enough to conclude that TOC availability can fully
411 explain the Hg signals observed in Lake Prespa throughout the 90-kyr succession.

412 Correlations between Hg_T, detrital mineral and/or TS availability are also largely absent, suggesting
413 that the complex Hg/TOC relationship is not a function of time-varying sulphides and detrital mineral
414 availability. Large peaks in Hg/K are visible during the Holocene (**Fig. 5**), but these are not reflected in
415 Hg_{AR} and therefore an artefact of considerably lower K concentrations within this section of the core
416 rather than indicators of changes in lake Hg levels. The highest positive r^2 value between Hg_T and TS
417 is observed during the Holocene (MIS 1: $r^2 = 0.25$) (**Fig. 4**), implying that >75 % of variance in the
418 dataset cannot be explained with sulphide availability during this time period. Correlations for other
419 periods are even weaker and some periods appear to show distinct patterns of Hg and potential host-
420 phase behaviour (**Fig. 4**).

421 One possibility is that Hg signals reflect changes in the dominant sources of organic and detrital
422 materials deposited in the lake. For example, combined isotopic and sedimentological data record
423 episodes of stronger algal blooms during MIS 1 and 5 (Leng et al., 2013), supported by coeval
424 abundance of freshwater diatom genera such as *Cyclotella* and *Aulacoseira* (Cvetkoska et al., 2015).
425 All correspond to elevated Hg_T, and so could imply more effective Hg burial by autochthonous organic
426 material compared to allochthonous (Leng et al., 2013; Damaschke et al., 2013). However, in the
427 presence of abundant binding ligands such as for the Lake Prespa record, maximum Hg burial is
428 limited principally by supply regardless of productivity, and so changing Hg signals in Lake Prespa
429 more likely reflect changes in environmental Hg availability; resulting from externally-driven
430 oscillations in Hg emission and/or exchange between (local) surface reservoirs such as forests, water
431 courses, and soils (Bishop et al., 2020; Obrist et al., 2018)). This interpretation is supported by the
432 lack of a close statistical correspondence between Hg, organic matter, sulphur, or detrital mineral
433 content, source, or composition (**Fig. 4**), which suggests that Hg burial efficiency is only weakly
434 associated with host phase availability in this system.

435

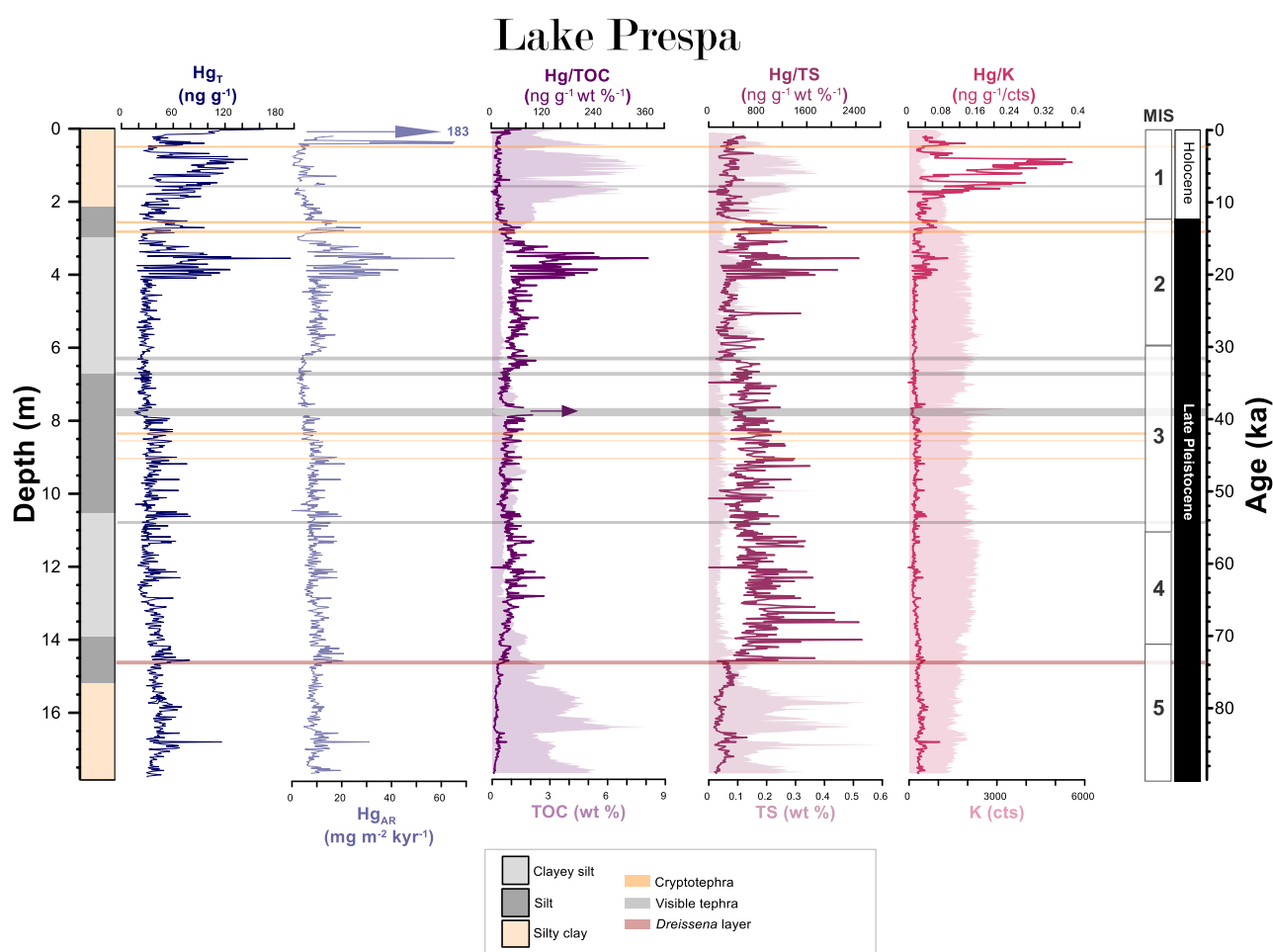


Figure 5: Total Hg (Hg_T) and total Hg accumulation rate (Hg_{AR}) for core Co1215 from Lake Prespa, presented as a function of depth and time, and relative to lithofacies, visible (grey shading) and cryptotephra (orange shading) layers. We include records of Hg_T (this study) normalized to records of total organic carbon (TOC) (Damaschke et al., 2013), total sulphur (TS) (Aufgebauer et al., 2012), and detrital mineral abundance (estimated by potassium (K)) (Panagiotopoulos et al., 2014), with filled shading marking the original datasets. A distinct lake low stand based on seismic profiles and sedimentological data is marked at 14.63 - 14.58 m depth (red shading) (Wagner et al., 2014a). A purple arrow marks sections where artificially high Hg/TOC values are generated by a sharp drop to near-zero TOC (<0.06 wt %) coinciding with deposition of the Y-5 (17.1 m) tephra unit – an effect expected as background sedimentation is interrupted by volcanic ash deposition. White boxes mark the marine isotope stages defined by (Lisiecki and Raymo, 2005), and stratigraphic periods are labelled in black/white.

436

437 Core 5045-1 from Lake Ohrid shows elevated Hg_T during the late Pleistocene compared to the
 438 Holocene (**Fig. 6; Table 1**). Peaks in Hg_T most consistently correspond to increases in K (detrital
 439 mineral) intensities, reflected in a broadly positive relationship between Hg_T and K throughout the
 440 succession (**Fig. 4, S3**). However, this relationship is only described by r^2 values <0.5 and the
 441 strength of this correlation varies across the span of the record, weakening during the Holocene (**Fig.**
 442 **4**).

443 Variable Hg values in the Ohrid record appear less influenced by organic matter and/or sulphide
 444 availability. Fluctuations in TOC/TS values suggest that some sulphide formation may have occurred
 445 during the late Pleistocene (MIS 2-5) (Wagner et al., 2009; Francke et al., 2016). However, even in
 446 these phases, TS remains low and correlations between Hg_T and TS are generally negative or weak
 447 ($r^2 < 0.2$; **Fig. 4**) so that Hg signals do not change in magnitude or expression even when TS

448 variability is accounted for (**Fig. 6**), potentially due to the oligotrophic state of Lake Ohrid favouring
 449 burial of sulphide-depleted sediments (Francke et al., 2016; Vogel et al., 2010). More remarkable, the
 450 relationship between Hg_T and organic matter in Lake Ohrid also shows an inverse correlation (**Fig. 4**).
 451 These trends may be explained by a scenario where the Hg flux to Ohrid from direct deposition and/or
 452 surrounding catchment is typically the limiting factor, rather than availability of potential host phases.

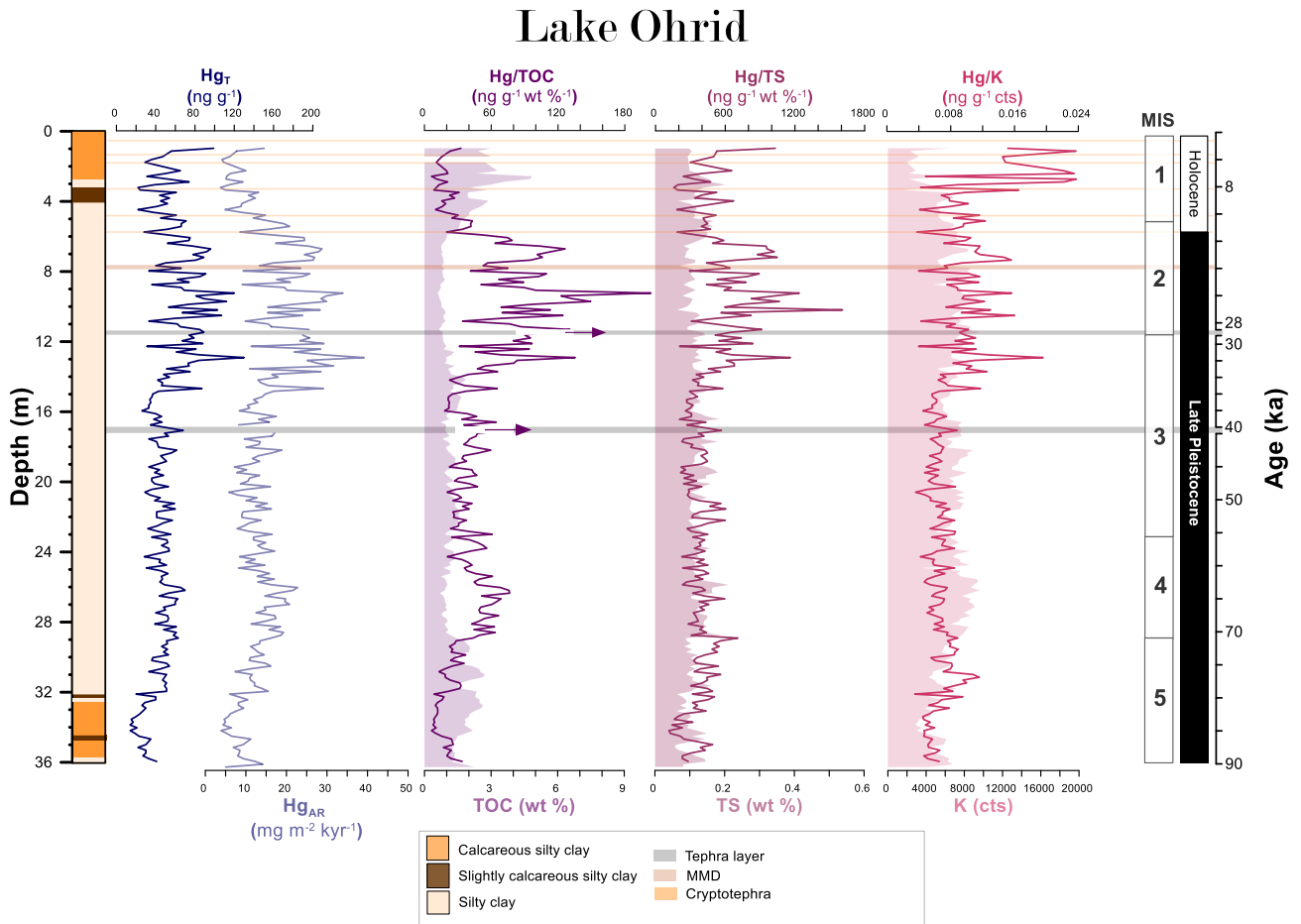


Figure 6: Total Hg (Hg_T) and total Hg accumulation rate (Hg_{AR}) for core 5045-1 from Lake Ohrid, presented as a function of depth and time, and relative to lithofacies, visible (grey shading) and cryptotephra (orange shading) layers. We include records of Hg_T (this study) normalized to records of total organic carbon (TOC) (Francke et al., 2016), sulphide (estimated by total sulphur (TS)) (Francke et al., 2016), and detrital mineral abundance (estimated by potassium (K)) (Francke et al., 2016; Wagner et al., 2019), with filled shading marking the original datasets. A mass movement deposit (MMD) is marked at 7.87 m depth (brown shading) (Francke et al., 2016). Purple arrows mark sections where artificially high Hg/TOC values are generated by a sharp drop to near-zero TOC ($<0.06\ wt\ \%$) coinciding with deposition of the Y-5 (17.1 m) and Mercato (11.5 m) tephra layers – an effect expected as background sedimentation is interrupted by volcanic ash deposition. White boxes mark the marine isotope stages as defined by Lisiecki and Raymo (2005), and stratigraphic periods are labelled in black/white.

453

454 Lake Ohrid and Lake Prespa show distinct differences in the strength of their Hg-host phase
 455 relationships. In Lake Prespa, Hg broadly covaries with organic matter (TOC), whereas in Lake Ohrid
 456 correlations are observed between Hg and detrital minerals (K). Nonetheless, only a relatively small
 457 proportion of Hg variability can be explained by host phase availability in each record. This suggests
 458 that while host phase availability may, at times, exert an influence on the Hg signals recorded in these
 459 lakes, the catchment-controlled changes in Hg fluxes are typically the more dominant effect on Hg in
 460 these sediment records. In the absence of a pronounced host-phase influence, retention of a
 461 measurable Hg signal requires that the net influx of Hg into the lake (e.g., surface runoff, wet/dry

462 deposition) exceeds the amount leaving the system due to processes such as runoff or evasion.
463 Therefore, we surmise that the Hg_T and Hg_{AR} signals recorded in Lake Prespa and Lake Ohrid are
464 records of net Hg input to the two lakes rather than the efficiency of sedimentary drawdown.

465

466 **4.2. Tephra layers**

467 As volcanic eruptions are among the most significant natural Hg sources, we assess whether the
468 previously recognized tephra deposition events in Lake Prespa correspond to changes in Hg
469 deposition. Overall, we find that individual tephra horizons and surrounding sediments do not
470 consistently correspond to measurable peaks in Hg_T or Hg_{AR} in Lake Prespa (**Fig. 5**). Only two of the
471 eleven preserved ash layers coincide with elevated Hg_T : Mercato (8.54 ± 0.09 ka; Somma-Vesuvius),
472 and LN1 (14.75 ± 0.52 ka; Campi Flegrei). These two units are not associated with disproportionately
473 large tephra volumes and neither coincide with evidence for transient changes in authigenic
474 carbonate precipitation or sediment diagenesis that may impact sedimentary Hg. This implies that Hg
475 concentrations in Lake Prespa cannot, in general, be unequivocally linked to short-lived (<1-year)
476 individual eruption events between ~90 and 0 ka (**Fig. S5**).

477 Discrete ash fall events (recorded by tephra/cryptotephra) do not consistently correspond to
478 measurable peaks in Hg_T or Hg_{AR} in the slightly lower-resolution (~400-yr per sample) Lake Ohrid
479 record (**Fig. S5**). Considering this lack of correspondence of Hg with ash layers, in conjunction with
480 the Lake Prespa data too, suggests that (a) surface Hg loading was not appreciably increased with
481 most large eruption events over the past 90 kyr in the Balkans and/or (b) sampling resolution may
482 need to be significantly higher and/or focused on lesser-bioturbated records to identify single, short-
483 lived volcanogenic perturbations of the scale and type occurring during the period recorded in the
484 Ohrid (and Prespa) sedimentary successions.

485

486 4.3. Variability through time

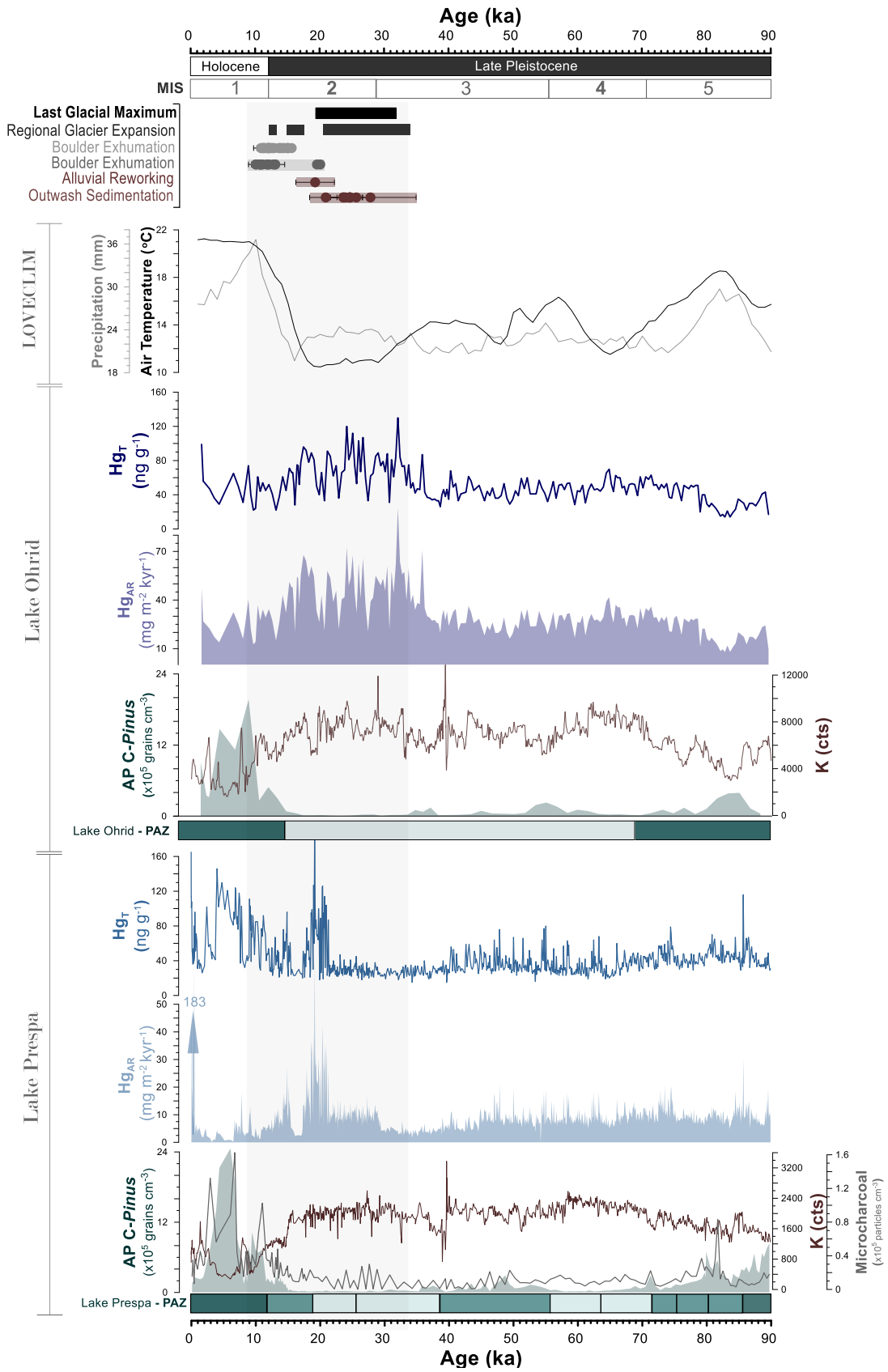


Figure 7: Total mercury (Hg_T) and mercury accumulation rate (Hg_{AR}) records for Lake Prespa and Lake Ohrid generated by this study and proxy datasets generated by prior studies. For Lake Prespa, these include arboreal pollen (AP) concentrations (Panagiotopoulos et al., 2014), microcharcoal (Panagiotopoulos, 2013), potassium (K) (Aufgebauer et al., 2012; Wagner et al., 2010), and pollen assemblage zones (PAZ) (Panagiotopoulos et al., 2014). For Lake Ohrid, these include AP concentrations (Sadori et al., 2016), potassium (K) (Wagner et al., 2019; Francke et al., 2016), 1000-year average surface-air temperature (SAT - °C) and annual mean precipitation (millimetres) both simulated by the LOVECLIM Earth system model (Goosse et al., 2010) for the Prespa/Ohrid region (Wagner et al., 2019), and pollen assemblage zones (PAZ) (Sadori et al., 2016). Pollen assemblage zones defined by Panagiotopoulos et al. (2014) (Lake Prespa) and Sadori et al. (2016) (Lake Ohrid) are presented as green bars, shaded relative to tree population density (darker colour = higher density). We include a chronology of glacial processes based on radiometric dating of glacial landforms in the following locations: the Voidomaitis river basin (purple) (Lewin et al., 1991; Woodward et al., 2008), the Pindus Mountains (lilac) (Allard et al., 2021, 2020; Styllas et al., 2018; Hughes et al., 2006; Pope et al., 2017), and the Dinaric Alps (blue) (Gromig et al., 2018; Ribolini et al., 2018; Ruzsiccizay-Rüdiger et al., 2020). White boxes mark the marine isotope stages (MIS) as defined by Lisiecki and Raymo (2005), and stratigraphic periods are labelled in black/white. Vertical grey shading denotes the timing of the largest changes in glacier extent and volume.

487

488 **4.3.1. Late Pleistocene (90 – 35 ka; MIS 5 to MIS3)**

489 The Lake Prespa and Lake Ohrid sediment cores show similarly muted variability in Hg_T and Hg_{AR}
490 values between ~90 and 35 ka (broadly MIS 5a-c, 4 & 3), alluding to relatively stable Hg inputs (**Fig.**
491 **7; Table 1**). High organic and low clastic material concentrations point to warmer climate conditions
492 during this interval, in which both catchments experienced an increase in moisture availability,
493 pronounced forest expansion, and plant diversification – collectively acting to stabilize hillslopes and
494 reduce deep soil erosion (Francke et al., 2019; Panagiotopoulos et al., 2014; Sadori et al., 2016,
495 2016). One possibility is that Hg sequestration during this interval was controlled by consistent rates
496 of algal scavenging (Biester et al., 2018; Outridge et al., 2007, 2019; Stern et al., 2009). Elevated
497 TOC (**Fig. 5**), hydrogen index, TOC/TN, and biogenic carbonate concentrations between ~90 and 71
498 ka in both Lake Prespa and Lake Ohrid signal nutrient upwelling and increased allochthonous inputs,
499 in conjunction with elevated primary productivity. For example, Lake Prespa records green algae
500 accumulation (Cvetkoska et al., 2016, 2015; Leng et al., 2013; Panagiotopoulos et al., 2014), and
501 sediments rich in biogenic silica ($bSiO_2$) are also evident in Lake Ohrid (Francke et al., 2016). Slow
502 changes in lake geochemistry associated with these biological processes are consistent with a steady
503 Hg_{AR} in both Lake Prespa and Lake Ohrid during this time, and absence of any especially pronounced
504 changes in Hg_T . This could suggest that, for a relatively prolonged period (~96–35 ka), Hg flux to the
505 two lakes did not change with a magnitude sufficient to cause measurable sedimentary changes, and
506 processes capable of amplifying differences in sedimentary Hg between Ohrid and Prespa were not
507 particularly influential.

508 MIS 3 marks the start of slow divergence between the Hg records of Lake Prespa and Lake Ohrid.
509 During MIS 3, proxy records suggest that conditions in the Prespa/Ohrid region were milder than MIS
510 4, but cooler and drier than MIS 5 (**Fig. 7**) (Panagiotopoulos et al., 2014; Sadori et al., 2016; Wagner
511 et al., 2019). Divergent Hg signals could be linked to two climate-driven processes. First, a reduction
512 in primary productivity in Lake Prespa signalled by decreasing TOC, hydrogen index, and endogenic
513 carbonate compared to values observed during MIS 5 (Aufgebauer et al., 2012; Cvetkoska et al.,

514 2016; Leng et al., 2013). Second is an increase in detrital material flux to both lakes (signalled by
515 elevated K count; **Fig. 7**), due to recession of the surrounding forests and subsequently elevated
516 rates of catchment erosion (Damaschke et al., 2013; Francke et al., 2019; Panagiotopoulos et al.,
517 2014; Sadori et al., 2016). This environmental shift is more likely to favour enhanced Hg mobility in
518 the catchment and burial in a system whereby detrital minerals could either constitute the primary
519 host phase or correlate to Hg_T; and so could explain the progressive elevation in Hg_T and Hg_{AR}
520 observed in Lake Ohrid (**Fig. 4**).

521

522 **4.3.2. Last Glaciation (35–12 ka; MIS 3 to MIS2)**

523 The timing, amplitude, and expression of Hg signals captured in Lake Prespa and Lake Ohrid change
524 significantly between ~35 and 12 ka (**Fig. 7**). The largest Hg_T and Hg_{AR} peaks in Lake Ohrid coincide
525 with the Last Glacial Maximum (LGM), and begin at ~35 ka (**Fig. 7**). Synchronous enrichments in K,
526 quartz, and Ti (Francke et al., 2016; Wagner et al., 2019) provide evidence for elevated clastic
527 terrigenous matter inputs and erosion, and are consistent with evidence for a significantly less-
528 vegetated catchment (Donders et al., 2021; Sadori et al., 2016). High clastic fluxes into the lake
529 during the LGM could also relate to meltwater run-off from local mountain glaciers (Ribolini et al.,
530 2011), which would transport large volumes of sediment generated by glacial abrasion, quarrying and
531 plucking (Carrivick and Tweed, 2021; Overeem et al., 2017) into the lake basin. Given that Hg
532 sequestration in Lake Ohrid appears partially related to the abundance of detrital minerals for much of
533 the record (**Fig. 4, 5**), these Hg peaks could relate to local, climate-driven shifts in landscape structure
534 associated with glaciation during MIS 2 (**Fig. 4, 7**).

535 Alternatively or in addition to these local effects, atmospheric mineral dust concentrations were also
536 up to twenty-times higher during the LGM (Simonsen et al., 2019). Mineral dust may be the most
537 important Hg carrier in ice-cores (Jitaru et al., 2009; Vandal et al., 1993), and studies have shown
538 evidence for notable redistribution of terrestrial Hg during the LGM owing to changes in regional
539 atmospheric dust deposition (de Lacerda et al., 2017; Fadina et al., 2019; Pérez-Rodríguez et al.,
540 2015). However, we see no clear evidence atmospheric dust played a major (direct) role in the local
541 Hg cycle in our data. For example, peaks in elemental ratios typically associated with mineral dust
542 deposits (e.g., Zr/Ti) do not correspond to peaks in Hg_T and/or Hg_{AR} (**Fig. S7**) (Vogel et al., 2010), nor
543 loess-based evidence for elevated aeolian dust fluxes over Central Europe and the Balkans during
544 the last glacial maximum (Újvári et al., 2010; Rousseau et al., 2021). Marine sediment records also do
545 not capture measurable changes in Saharan dust influx to the Ionian and Aegean seas corresponding
546 to pronounced Hg signals in Lake Ohrid (**Fig. S7**) (Ehrmann and Schmiedl, 2021). Therefore, we
547 cannot mechanistically link elevated Hg values during MIS 2 in Lake Ohrid to broad-scale changes in
548 atmospheric dust deposition.

549 The largest Hg_T and Hg_{AR} peaks in Lake Prespa occur between 21.3 ± 1.7 (1σ from the Bayesian age
550 model, see **Fig. 3**) ka and 17.5 ± 0.7 ka. These signals do not correspond to a measurable change in
551 host phase availability (**Fig. 5**), so it is unlikely that these peaks reflect changes in TOC, TS, and/or K.

552 However, they do coincide with deglaciation of the Pindus and Dinaric mountains (**Fig. 7**) (Hughes et
553 al., 2023). Geomorphological evidence suggests that glaciers were present across the Prespa/Ohrid
554 region between ~26.5 and 15 ka (Belmecheri et al., 2009; Gromig et al., 2018; Ribolini et al., 2018;
555 Ruzkiczay-Rüdiger et al., 2020), and indeed that periglacial processes created a landscape
556 characterized by intense weathering, erosion and sediment transport (Hughes and Woodward, 2017;
557 Allard et al., 2021). Glacial meltwaters thus likely constituted a major source of water input to Lake
558 Prespa during the last deglaciation. Glaciers are important sinks for atmospheric Hg deposited by
559 both dry and wet processes (Durnford and Dastoor, 2011; Zhang et al., 2012), and large quantities of
560 Hg can accumulate in organic-rich frozen soils (permafrost, Schuster et al., 2018). High proportions of
561 detrital matter within glacial ice, snow, and organic matter facilitate the effective, long-term (>100s-
562 1000s of years) retention of atmospheric Hg, meaning that rapid snow/ice melt and permafrost
563 thawing can produce transient 'pulses' of Hg into lakes without a comparable peak in sediment influx
564 (Durnford and Dastoor, 2011; Kohler et al., 2022). This is consistent with the abrupt and short-lived
565 increase in Hg concentration retained in Lake Prespa between 21.3 and 17.5 (± 1.7 – 0.7 (1σ)) ka,
566 which occurs in the absence of a pronounced change in terrigenous elements (e.g., Ti, Rb) or TS
567 (**Fig. 5, 7**).

568 Lakes Ohrid and Prespa show two other striking differences in Hg concentration between 35–12 ka
569 (**Fig. 7**). First, Lake Prespa does not record a distinct Hg_T or Hg_{AR} signal during the LGM, and second,
570 Lake Ohrid does not record a distinct Hg_T or Hg_{AR} signal corresponding to deglaciation. Given their
571 close proximity and environmental similarity, both lakes could be expected to record similar overall
572 signals if the climate-driven processes influencing Hg_{AR} were broadly similar. One plausible
573 explanation could be a disproportionately large change in Lake Prespa's total volume compared to
574 Lake Ohrid. Increased abundance of small *Fragilariaceae* and benthic *Eolimna submuralis* diatom
575 species point to generally low temperatures and lake levels during MIS 2 (Cvetkoska et al., 2015).
576 These conditions are also indicated by elevated concentrations of ice-rafted coarse sand and gravel
577 grains, and further suggest persistent ice formation on the lake surface, likely facilitated by the lake's
578 shallow depth (Damaschke et al., 2013; Wagner et al., 2010; Vogel et al., 2010). It is possible that the
579 heightened presence of ice at the peak of glaciation served as a natural barrier between the surface
580 and the sediments of Lake Prespa, effectively slowing the net flux of Hg into delivery of solutes to the
581 basin. A simultaneous lack of ice cover on Lake Ohrid, linked to greater water depths, could also
582 justify why Hg_{AR} remained high in this lake during the LGM, as the Hg influx pathway would be
583 unaffected by ice formation (**Fig. 7**).

584 Water volume changes may have also influenced the hydrological connection between lakes Ohrid
585 and Prespa during deglaciation (Cvetkoska et al., 2016; Jovanovska et al., 2016; Leng et al., 2010).
586 Tracer experiments and stable isotope ($\delta^{18}O$) analysis suggest that water draining from Lake Prespa
587 accounts for a significant proportion of Lake Ohrid's water inflow alongside precipitation (Matzinger et
588 al., 2006; Wagner et al., 2010; Lacey and Jones, 2018), with high rates of prior calcite precipitation
589 occurring in the connecting karst system (Eftimi et al., 1999; Leng et al., 2010; Matzinger et al., 2006).
590 However, a change to lower $\delta^{18}O$ of lakewater and TIC in both lakes during the last glaciation point to

591 a reduction in the contribution of karst-fed waters to Lake Ohrid (Lacey et al., 2016; Leng et al., 2013).
592 Although it is unlikely that the two hydrological systems became completely decoupled (Belmecheri et
593 al., 2009; Lézine et al., 2010), evidence for permafrost formation at high elevations between 35 and
594 18 ka (Oliva et al., 2018) and lower precipitation could be linked to a reduction in karst aquifer activity
595 (**Fig. 7**). For shallower Lake Prespa, lower precipitation may also have led to a larger reduction in lake
596 volume compared to Lake Ohrid, decrease in the number (and pressure) of active sinkholes, and
597 subsequently the outflow of water and solutes (e.g., Hg) into Lake Ohrid (Wagner et al., 2014a) –
598 increasing both Hg_T and Hg_{AR}. Together, the collective impact of disproportionately large, climate-
599 driven reductions in water level could explain why rates of Hg accumulation were significantly higher
600 in Lake Prespa during deglaciation compared to the LGM. Glacial meltwaters would elevate the net
601 Hg input compared to the LGM, and reduced ice cover would permit a more direct pathway for Hg to
602 be delivered into the basin; both processes becoming effective while underground permafrost
603 continued to limit the intra-basin exchange of water and solutes.

604 Neither Lake Ohrid nor Lake Prespa show large changes in Hg concentration nor accumulation during
605 the Oldest (17.5-14.5 ka) and Younger (12.9-11.7 ka) Dryas. Both lakes contain clear evidence for an
606 abrupt return to glacial conditions during this time. Lake Prespa sediments record shifts in tree pollen
607 and diatom assemblages alluding to a net reduction in local winter temperatures and moisture
608 availability (Aufgebauer et al., 2012a; Panagiotopoulos et al., 2013; Cvetkoska et al., 2014), and high
609 uranium (²³⁴U/²³⁸U) activity ratios, low tree pollen percentages, and low TIC concentrations in Lake
610 Ohrid also pertain to intense hillslope erosion owing to a more open catchment structure (Francke et
611 al., 2019b; Lézine et al., 2010). Geomorphological evidence also pertains to local glacier stabilization
612 (Gromig et al., 2018; Ribolini et al., 2018; Ruszkiczay-Rüdiger et al., 2020) (**Fig. 7**). Nonetheless, we
613 suggest these events may have been too (a) short-lived, and/or (b) climatically mild to produce a
614 similarly distinct response in the terrestrial Hg cycle as the processes operating during, and
615 immediately following, the LGM; potentially explaining the lack of an associated sedimentary Hg
616 signal.

617

618 **4.3.3. Holocene (12–0 ka; MIS 1)**

619 The timing and amplitude of Hg_T and Hg_{AR} signals recorded in Lake Prespa and Lake Ohrid
620 sediments are noticeably different during the Holocene (MIS 1). Between 12±0.5 and 3±0.2 ka, Lake
621 Prespa captures a series of large peaks in Hg_T and Hg_{AR}, corresponding to high TOC and TIC
622 indicative of elevated productivity, higher rates of organic material preservation, and limited mixing
623 (**Fig. 5**). Conversely, Hg_T and Hg_{AR} show a progressive decline in Lake Ohrid during MIS 1, despite
624 coeval increases in TOC and TIC (**Fig. 6**). These observations suggest that for most of the Holocene
625 Hg fluxes into the two lakes were largely decoupled, likely due to differences in catchment and basin
626 dynamics which impacted the rate of Hg delivery to (and burial in) the lakes.

627 Divergent Hg signals in Lake Ohrid and Lake Prespa during this time may be linked to heightened
628 wildfire frequency and/or intensity. Wildfires have the capacity to (in)directly release Hg from

629 vegetation, and/or through associated changes in soil erosion. Proxy evidence alludes to interglacial
630 conditions characterised by heightened seasonality, characterized by very warm, dry summers
631 coupled with wet, mild winters, an overall increase in the prevalence of deciduous tree species
632 (Cvetkoska et al., 2014; Panagiotopoulos, 2013); but also an increase in macro and microcharcoal
633 concentrations in Lake Prespa (**Fig.7**; Panagiotopoulos et al. 2013). Large wildfires would have a
634 broadly regional-scale impact which, given the close proximity of our two lakes, could theoretically
635 produce a measurable Hg signal in both systems. However, more frequent and/or intense regional
636 fires could also yield measurably different sedimentary Hg signals by their capacity to: (1) enhance
637 surface run off without a corresponding increase in erosion and effectively reduce transport of
638 catchment sourced, mineral-hosted Hg (Mataix-Solera et al., 2011; Shakesby, 2011); (2) enhance
639 downstream transport of Hg released from burned soils and bound to fine and coarse particulate
640 matter (Burke et al., 2010; Takenaka et al., 2021); and/or (3) release large quantities of Hg into the
641 atmosphere following biomass combustion (Howard et al., 2019; Melendez-Perez et al., 2014;
642 Roshan and Biswas, 2023). All three combine to generate impacts that may vary in significance owing
643 to lake-specific differences in sedimentation, accumulation, and flux of materials to/from the lake.

644 An increase in wildfire activity also corresponds to a period of intensifying human influence in the
645 region; predominantly in the form of land use change, agriculture, and animal husbandry (Cvetkoska
646 et al., 2014; Masi et al., 2018; Panagiotopoulos et al., 2013; Rothacker et al., 2018; Thienemann et
647 al., 2017; Wagner et al., 2009). Widespread mineral resource exploitation and metalworking on the
648 Balkan peninsula is recorded as early as ~8 ka (Gajić-Kvaščev et al., 2012; Longman et al., 2018;
649 Radivojević and Roberts, 2021; Schotsmans et al., 2022), and release of detrital Hg during cinnabar
650 ore extraction and use of Hg in gold extraction (amalgamation) has been linked to pronounced Hg
651 contamination in modern sedimentary units in the region (Covelli et al., 2001; Fitzgerald and Lamborg,
652 2013). Directly quantifying the influence of (hydro)climate- versus human-driven impacts on
653 sedimentary Hg records presents a major challenge as these factors are interdependent.
654 Nonetheless, these factors could produce a more measurable effect in lake systems with heightened
655 sensitivity to changes in water, nutrient and pollutant fluxes. This could explain why large Hg signals
656 are observed in Lake Prespa between ~12 and 3 ka but not Lake Ohrid: Lake Prespa is shallow
657 relative to its surface area (**Fig. 2**), meaning that relatively small oscillations in pollutant influxes can
658 lead to appreciable changes in lake geochemistry (Cvetkoska et al., 2015; Matzinger et al., 2006).

659 Decoupling of the two Hg records effectively disappears ~3 ka ago, where both lakes show a sharp
660 and pronounced rise in Hg_T and Hg_{AR} (**Fig. 7**). Several lines of evidence point to human activity as the
661 primary cause. On a local scale, a rapid increase in the biological productivity (eutrophication) of Lake
662 Prespa since ~1.6 (±0.06) ka alludes to greater disturbance of catchment soils by agricultural
663 practices, and eventually use of inorganic compounds such as pesticides and fertilizers (Aufgebauer
664 et al., 2012; Cvetkoska et al., 2014; Krstić et al., 2012; Leng et al., 2013). Signals observed in **Figure**
665 **7** may thus be a product of human-induced changes in organic or minerogenic material flux: each
666 facilitating more efficient delivery of catchment-sourced Hg (Fitzgerald et al., 2005), and possibly also
667 stimulating microbial Hg methylation within the sediment (Soerensen et al., 2016). On a broader scale

668 peaks in Hg_T and Hg_{AR} correspond to a sustained rise in European and/or global Hg emissions, owing
669 to increased deforestation, fossil fuel extraction and combustion, and intentional use of Hg for
670 resource extraction/production (Outridge et al., 2018; United Nations Environment Programme, 2018).
671 An increasing number of sedimentary archives record Hg enrichments as early as ~3 ka ago
672 (Biskaborn et al., 2021; Guédron et al., 2019; Li et al., 2020; Pan et al., 2020). The emergence of
673 simultaneous Hg_T and Hg_{AR} peaks in Lakes Ohrid and Prespa following ~3 ka underscores the
674 magnitude and global distribution of this change in Hg sources and emissions (**Fig. 7**), and point to a
675 rise in Hg fluxes between 3 and 0 ka that was distinct enough to effectively overwhelm previously
676 dominant natural drivers of Hg variability.

677

678 **4.4. Key differences & implications**

679 The magnitude and expression of Hg signals recorded in Lake Prespa and Lake Ohrid are different in
680 three aspects. First, the extent to which different host phases can (or cannot) explain time-varying
681 patterns in Hg concentration differs between the two lakes. Although only a limited fraction of Hg
682 variability in either record can be explained by availability of any single host phase, the low degree of
683 covariance that we do observe points to organic material playing the most significant role as a Hg
684 host in Lake Prespa. In contrast, Hg correlates most strongly with detrital minerals in Lake Ohrid over
685 the same period (0-90 ka) (**Fig. 4**). The second difference is visible during the last glaciation (~35–12
686 ka): in Lake Ohrid Hg concentrations peak during the LGM (35.8–12 ka), whereas Lake Prespa
687 captures transient, high-amplitude peaks during deglaciation, starting ~15-kyr later (**Fig. 7**). The third
688 difference is visible during the Holocene. The largest signals in the entire Lake Prespa record are
689 observed between ~8 and 0 ka, whereas Hg concentrations do not increase in Lake Ohrid until ~2 ka.
690 These observations raise the question: *for two lakes located in such close geographical proximity and*
691 *having experienced similar climate conditions, what may have caused such pronounced differences*
692 *from ~35 ka (**Fig. 2**)?*

693 Differences in bathymetric structure may offer a plausible explanation. For example, the largest
694 changes in the amplitude and frequency of peaks in Hg_T and Hg_{AR} are exhibited by Lake Prespa (**Fig.**
695 **7**): a shallow basin that contains >90 % less water than Lake Ohrid, despite only a ~30 % difference
696 in surface area (Wagner et al., 2010). Increased distance from lake margin to core site in Lake Ohrid
697 would mean distribution of material over a greater total area, and thus more time for net Hg loss to
698 occur either by evasion from the water surface (Cooke et al., 2020), removal of water (and suspended
699 material) via riverine outlets (Bishop et al., 2020), or processes taking place within the water column
700 (Frieling et al., 2023) prior to burial. Therefore, preservation of a measurable Hg signal in a deep lake
701 (e.g., Lake Ohrid) would require notably larger influx of Hg, and this sedimentary signal would also
702 likely be significantly smaller than the equivalent 'dose' delivered to a smaller and/or shallower lake
703 (e.g., Lake Prespa). Coupled with evidence for high-amplitude fluctuations in lake water δ¹⁸O (±6‰)
704 (Leng et al., 2010) and lake level (Cvetkoska et al., 2015, 2016) corresponding to pronounced Hg

705 variability in Lake Prespa, but not in Lake Ohrid (**Fig. 7**), our data suggest that smaller, shallower
706 lakes may be particularly sensitive recorders of transient, changes in Hg fluxes.

707 Divergent bathymetric structures are also linked to distinct differences in biological composition and
708 nutrient availability in lakes Ohrid and Prespa. The deep (~240 m) waters of Lake Ohrid host a highly
709 oligotrophic (nutrient poor) environment characterized by low levels of biological productivity, and a
710 high abundance of planktonic diatom species (e.g., *Cyclotella*) (Cvetkoska et al., 2021). Conversely,
711 Lake Prespa's shallower (~14 m) waters host a dominantly mesotrophic (nutrient-rich) system in
712 which benthic and planktonic diatom species are present in equal abundance (Jovanovska et al.,
713 2016; Cvetkoska et al., 2016), and allude to moderate/high biological productivity (Leng et al., 2013).
714 Productivity is a potentially important factor influencing the Hg composition of lake sediment: high
715 productivity typically favours higher concentrations of algal biomass, allowing for more effective Hg
716 scavenging by organic particles and export to the sediment (Biestler et al., 2018; Soerensen et al.,
717 2016; Hermanns et al., 2013). While the overall signal will remain dominated by Hg availability, broad-
718 scale differences in productivity between lakes Prespa and Ohrid through time could provide an
719 additional explanation for the disparate expression of recorded Hg signals (**section 4.1**); with notably
720 higher productivity in the shallower Lake Prespa further increasing its sensitivity to changes in nutrient
721 status, erosion, and hydrology.

722 Local differences in Hg emission by neotectonic activity may have also contributed to the divergent
723 Hg signals, owing to differences in the host rock geology, tectonic instability, and mechanical stress
724 regimes of faults surrounding the two basins (Hoffmann et al., 2010; Lindhorst et al., 2015). However,
725 the significance of these differences cannot be fully assessed in the absence of direct Hg emission
726 measurements (see **Text SD4**).

727 The two records presented here highlight that Hg cycling in lacustrine environments is distinct from
728 open marine systems. In marine systems, Hg fluxes can be broadly modulated by large-scale
729 continental sediment (Fadina et al., 2019; Figueiredo et al., 2022; Kita et al., 2016) and/or
730 atmospheric inputs (Chede et al., 2022), and Hg burial flux ultimately becomes more closely related to
731 host-phase availability. Conversely, both Lake Prespa and Lake Ohrid highlight how the local basin
732 and catchment characteristics both exert a key control on the delivery of Hg to lacustrine sediments,
733 and suggest that differences in Hg cycling between geographically-proximal basins could occur as a
734 function of diverse physical, hydrological, and biological properties.

735 Our observations highlight that multi-millennial lacustrine Hg records allow a different perspective of
736 the Hg cycle compared to marine records, and, for example, may be used to infer how local, regional
737 and global climatic conditions could have altered processes important to the terrestrial Hg cycle.
738 Because lacustrine records are much better suited to recording smaller-scale processes it is also
739 clear that extrapolating the (non-marine) Hg cycle response from a single lacustrine Hg record is
740 challenging. For example, a single-core approach could produce a large degree of uncertainty owing
741 to variable sediment focussing and catchment-sourced influx of organic and inorganic materials (Blais
742 and Kalff, 1995; Engstrom and Rose, 2013; Engstrom and Wright, 1984). A valuable next step would

743 be to apply a source-to-sink approach within a well-known lacustrine catchment: to assess the extent
744 to which Hg sedimentation is spatially heterogeneous within a lacustrine system, and whether multiple
745 cores extracted from different locations within the same basin would yield markedly different Hg
746 trends. Intra-basin heterogeneity in Hg sources, reactions, and transformations could also be
747 examined through measurement of stable Hg isotopes; particularly in millennia-scale sedimentary
748 records where the nature of these processes may change through time (Blum et al., 2014; Jiskra et
749 al., 2022; Kurz et al., 2019). Work of this nature would make great strides toward assessing how
750 representative of variability in the local Hg cycle a single, in this case, lake core is, and whether intra-
751 basin fluctuations in sedimentation, resuspension, and erosion could translate to measurable changes
752 in sedimentary Hg burial.

753 Past changes in environmental Hg availability inferred from sedimentary records have typically been
754 examined (and presented) by normalizing Hg to a dominant host phase, often taken as organic matter
755 (Fadina et al., 2019; Figueiredo et al., 2020; Grasby et al., 2019; Kita et al., 2016; Percival et al.,
756 2015). However, availability of organic matter or other host phases that scavenge Hg here appear to
757 represent just one of several processes governing Hg burial in lacustrine systems, and this process is
758 very likely systematically less significant compared to marine records in lieu of changes in catchment
759 and basin processes such as erosion, nutrient status, and hydrology (Outridge et al., 2019). Outside
760 pre-industrial times (or periods without an overwhelming global Hg cycle perturbation; such as during
761 LIP formation (Grasby et al., 2019)), a single common process/mechanism is therefore unlikely to
762 produce a unanimous stratigraphic signal across all lakes or even for two adjacent lakes as shown in
763 this study.

764

765 **6. Conclusions**

766 To better understand local and regional impact of climate, vegetation and catchment characteristics
767 on lacustrine Hg records, we present two new high-resolution, Hg records for the last ~90 kyr from
768 Lake Prespa and Lake Ohrid. The two records show some similarities but also distinct differences in
769 the strength of the relationships between Hg, TOC, TS, and detrital minerals (K), with only a relatively
770 small proportion of Hg variability attributable to host phase availability in each record. Our findings
771 provide three valuable insights. First, that local sedimentary environment does influence Hg burial.
772 Covariance with host phases accounts for a limited proportion of the observed variability, suggesting
773 that many of the Hg_T and Hg_{AR} signals recorded in Lake Prespa and Lake Ohrid reflect net Hg input to
774 the two lakes across timescales ranging from decades to multiple millennia. Second, Hg signals can
775 reflect changes in (and also differences between) catchment hydrology and structure. Despite their
776 proximity, the magnitude and expression of the recorded signals are considerably different between
777 Lake Prespa and Lake Ohrid, suggesting these inputs changed relative to sedimentary setting and in
778 response to changing interactions between the two systems. Finally, regional-scale climate variability
779 can measurably affect the Hg signals retained in lake sediments: both lakes Prespa and Ohrid
780 showing changes in Hg concentration and accumulation corresponding to glacial (late Pleistocene)

781 and interglacial (Holocene) climate conditions. It follows that local, regional, or global changes in
782 climate or hydrological cycling capable of affecting mineral soils, (peri-)glacial features or fire regime
783 in the lake catchment could all impact Hg fluxes. These findings prompt further examination of how
784 orbital-scale climate variability (>10³-year timescales) may influence the terrestrial Hg cycle, not only
785 to better resolve processes acting on single lacustrine and terrestrial successions, but also to identify
786 which of these (local) processes could hold relevance for Hg cycling on a global scale.

787

788 **Competing Interests**

789 The corresponding author declares that none of the authors have any competing interests.

790

791 **Acknowledgements**

792 ARP, IMF, JF, and TAM acknowledge funding from European Research Council Consolidator Grant
793 V-ECHO (ERC-2018-COG-818717-V-ECHO). ARP thanks Professor David Thomas and Mona
794 Edwards (School of Geography, Oxford) for logistical assistance with sample transfer and storage. KP
795 acknowledges funding from the German Research Foundation (DFG grant PA 2664/4-1). All authors
796 thank members of the Scientific Collaboration on Past Speciation Conditions in Lake Ohrid
797 (SCOPSCO), and the CRC 806 “*Our Way to Europe - Culture-Environment Interaction and Human*
798 *Mobility in the Late Quaternary*” projects: for their efforts in producing the Lake Ohrid and Lake
799 Prespa sediment successions, and making the data available for scientific use.

800

801 **References Cited**

802 Allard, J. L., Hughes, P. D., Woodward, J. C., Fink, D., Simon, K., and Wilcken, K. M.: Late Pleistocene glaciers in Greece: A
803 new 36Cl chronology, *Quaternary Science Reviews*, 245, 106528, <https://doi.org/10.1016/j.quascirev.2020.106528>, 2020.

804 Allard, J. L., Hughes, P. D., and Woodward, J. C.: A radiometric dating revolution and the Quaternary glacial history of the
805 Mediterranean mountains, *Earth-Science Reviews*, 223, 103844, <https://doi.org/10.1016/j.earscirev.2021.103844>, 2021.

806 Aufgebauer, A., Panagiotopoulos, K., Wagner, B., Schaebitz, F., Viehberg, F. A., Vogel, H., Zanchetta, G., Sulpizio, R., Leng,
807 M. J., and Damaschke, M.: Climate and environmental change in the Balkans over the last 17 ka recorded in sediments from
808 Lake Prespa (Albania/F.Y.R. of Macedonia/Greece), *Quaternary International*, 274, 122–135,
809 <https://doi.org/10.1016/j.quaint.2012.02.015>, 2012

810 Belmecheri, S., Namiotko, T., Robert, C., von Grafenstein, U., and Danielopol, D. L.: Climate controlled ostracod preservation
811 in Lake Ohrid (Albania, Macedonia), *Palaeogeography, Palaeoclimatology, Palaeoecology*, 277, 236–245,
812 <https://doi.org/10.1016/j.palaeo.2009.04.013>, 2009.

813 Benoit, J. M., Gilmour, C. C., Mason, R. P., and Heyes, A.: Sulfide controls on mercury speciation and bioavailability to
814 methylating bacteria in sediment pore water, *Environmental Science and Technology*, 33, 1780,
815 <https://doi.org/10.1021/es992007q>, 1999.

816 Biester, H., Pérez-Rodríguez, M., Gilfedder, B.-S., Martínez Cortizas, A., and Hermanns, Y.-M.: Solar irradiance and primary
817 productivity controlled mercury accumulation in sediments of a remote lake in the Southern Hemisphere during the past 4000

- 818 years: Primary productivity and mercury accumulation, *Limnol. Oceanogr.*, 63, 540–549, <https://doi.org/10.1002/lno.10647>,
819 2018.
- 820 Bin, C., Xiaoru, W., and Lee, F. S. C.: Pyrolysis coupled with atomic absorption spectrometry for the determination of mercury
821 in Chinese medicinal materials, *Analytica Chimica Acta*, 447, 161–169, [https://doi.org/10.1016/S0003-2670\(01\)01218-1](https://doi.org/10.1016/S0003-2670(01)01218-1), 2001.
- 822 Bini, M., Zanchetta, G., Perçoiu, A., Cartier, R., Català, A., Cacho, I., Dean, J. R., Di Rita, F., Drysdale, R. N., Finnè, M., Isola,
823 I., Jalali, B., Lirer, F., Magri, D., Masi, A., Marks, L., Mercuri, A. M., Peyron, O., Sadori, L., Sicre, M. A., Welc, F., Zielhofer, C.,
824 and Brisset, E.: The 4.2 ka BP Event in the Mediterranean region: An overview, *Climate of the Past*, 15, 555–577,
825 <https://doi.org/10.5194/cp-15-555-2019>, 2019.
- 826 Bishop, K., Shanley, J. B., Riscassi, A., de Wit, H. A., Eklöf, K., Meng, B., Mitchell, C., Osterwalder, S., Schuster, P. F.,
827 Webster, J., and Zhu, W.: Recent advances in understanding and measurement of mercury in the environment: Terrestrial Hg
828 cycling, *Science of the Total Environment*, 721, <https://doi.org/10.1016/j.scitotenv.2020.137647>, 2020.
- 829 Biskaborn, B. K., Narancic, B., Stoof-Leichsenring, K. R., Pestryakova, L. A., Appleby, P. G., Piliposian, G. T., and Diekmann,
830 B.: Effects of climate change and industrialization on Lake Bolshoe Toko, eastern Siberia, *J Paleolimnol*, 65, 335–352,
831 <https://doi.org/10.1007/s10933-021-00175-z>, 2021.
- 832 Blaauw, M. and Christeny, J. A.: Flexible paleoclimate age-depth models using an autoregressive gamma process, *Bayesian
833 Analysis*, 6, 457–474, <https://doi.org/10.1214/11-BA618>, 2011.
- 834 Blais, J. M. and Kalf, J.: The influence of lake morphometry on sediment focusing, *Limnol. Oceanogr.*, 40, 582–588,
835 <https://doi.org/10.4319/lo.1995.40.3.0582>, 1995.
- 836 Blum, J. D., Sherman, L. S., and Johnson, M. W.: Mercury Isotopes in Earth and Environmental Sciences, *Annu. Rev. Earth
837 Planet. Sci.*, 42, 249–269, <https://doi.org/10.1146/annurev-earth-050212-124107>, 2014.
- 838 Branfireun, B. A., Cosio, C., Poulain, A. J., Riise, G., and Bravo, A. G.: Mercury cycling in freshwater systems - An updated
839 conceptual model, *Science of the Total Environment*, 745, <https://doi.org/10.1016/j.scitotenv.2020.140906>, 2020.
- 840 Burke, M. P., Hogue, T. S., Ferreira, M., Mendez, C. B., Navarro, B., Lopez, S., and Jay, J. A.: The Effect of Wildfire on Soil
841 Mercury Concentrations in Southern California Watersheds, *Water Air Soil Pollut*, 212, 369–385,
842 <https://doi.org/10.1007/s11270-010-0351-y>, 2010.
- 843 Carrivick, J. L. and Tweed, F. S.: Deglaciation controls on sediment yield: Towards capturing spatio-temporal variability, *Earth-
844 Science Reviews*, 221, 103809, <https://doi.org/10.1016/j.earscirev.2021.103809>, 2021.
- 845 Chakraborty, P., Sarkar, A., Vudamala, K., Naik, R., and Nath, B. N.: Organic matter - A key factor in controlling mercury
846 distribution in estuarine sediment, *Marine Chemistry*, 173, 302–309, <https://doi.org/10.1016/j.marchem.2014.10.005>, 2015.
- 847 Chede, B. S., Venancio, I. M., Figueiredo, T. S., Albuquerque, A. L. S., and Silva-Filho, E. V.: Mercury deposition in the western
848 tropical South Atlantic during the last 70 ka, *Palaeogeography, Palaeoclimatology, Palaeoecology*, 601, 111122,
849 <https://doi.org/10.1016/j.palaeo.2022.111122>, 2022.
- 850 Cooke, C. A., Martínez-Cortizas, A., Bindler, R., and Sexauer Gustin, M.: Environmental archives of atmospheric Hg deposition
851 – A review, *Science of the Total Environment*, 709, 134800, <https://doi.org/10.1016/j.scitotenv.2019.134800>, 2020.
- 852 Cordeiro, R. C., Turcq, B., Sifeddine, A., Lacerda, L. D., Silva Filho, E. V., Gueiros, B., Potty, Y. P., Santelli, R. E., Pádua, E.
853 O., and Patchinelam, S. R.: Biogeochemical indicators of environmental changes from 50Ka to 10Ka in a humid region of the
854 Brazilian Amazon, *Palaeogeography, Palaeoclimatology, Palaeoecology*, 299, 426–436,
855 <https://doi.org/10.1016/j.palaeo.2010.11.021>, 2011.
- 856 Covelli, S., Faganeli, J., Horvat, M., and Brambati, A.: Mercury contamination of coastal sediments as the result of long-term
857 cinnabar mining activity (Gulf of Trieste, northern Adriatic sea), *Applied Geochemistry*, 16, 541–558,
858 [https://doi.org/10.1016/S0883-2927\(00\)00042-1](https://doi.org/10.1016/S0883-2927(00)00042-1), 2001.
- 859 Cvetkoska, A., Levkov, Z., Reed, J. M., and Wagner, B.: Late Glacial to Holocene climate change and human impact in the
860 Mediterranean: The last ca. 17ka diatom record of Lake Prespa (Macedonia/Albania/Greece), *Palaeogeography,
861 Palaeoclimatology, Palaeoecology*, 406, 22–32, <https://doi.org/10.1016/j.palaeo.2014.04.010>, 2014.
- 862 Cvetkoska, A., Levkov, Z., Reed, J. M., Wagner, B., Panagiotopoulos, K., Leng, M. J., and Lacey, J. H.: Quaternary climate
863 change and Heinrich events in the southern Balkans: Lake Prespa diatom palaeolimnology from the last interglacial to present,
864 *Journal of Paleolimnology*, 53, 215–231, <https://doi.org/10.1007/s10933-014-9821-3>, 2015.
- 865 Cvetkoska, A., Jovanovska, E., Francke, A., Tofilovska, S., Vogel, H., Levkov, Z., Donders, T. H., Wagner, B., and Wagner-
866 Cremer, F.: Ecosystem regimes and responses in a coupled ancient lake system from MIS 5b to present: the diatom record of
867 lakes Ohrid and Prespa, *Biogeosciences*, 13, 3147–3162, <https://doi.org/10.5194/bg-13-3147-2016>, 2016.

- 868 Cvetkoska, A., Jovanovska, E., Hauffe, T., Donders, T. H., Levkov, Z., Van De Waal, D. B., Reed, J. M., Francke, A., Vogel, H.,
869 Wilke, T., Wagner, B., and Wagner-Cremer, F.: Drivers of phytoplankton community structure change with ecosystem ontogeny
870 during the Quaternary, *Quaternary Science Reviews*, 265, 107046, <https://doi.org/10.1016/j.quascirev.2021.107046>, 2021.
- 871 Damaschke, M., Sulpizio, R., Zanchetta, G., Wagner, B., Böhm, A., Nowaczyk, N., Rethemeyer, J., and Hilgers, A.:
872 Tephrostratigraphic studies on a sediment core from Lake Prespa in the Balkans, *Climate of the Past*, 9, 267–287,
873 <https://doi.org/10.5194/cp-9-267-2013>, 2013.
- 874 Ding, X., Li, D., Zheng, L., Bao, H., Chen, H.-F., and Kao, S.-J.: Sulfur Geochemistry of a Lacustrine Record from Taiwan
875 Reveals Enhanced Marine Aerosol Input during the Early Holocene, *Sci Rep*, 6, 38989, <https://doi.org/10.1038/srep38989>,
876 2016.
- 877 Donders, T., Panagiotopoulos, K., Koutsodendris, A., Bertini, A., Mercuri, A. M., Masi, A., Combourieu-Nebout, N., Joannin, S.,
878 Kouli, K., Kousis, I., Peyron, O., Torri, P., Florenzano, A., Francke, A., Wagner, B., and Sadori, L.: 1.36 million years of
879 Mediterranean forest refugium dynamics in response to glacial-interglacial cycle strength, *Proceedings of the National
880 Academy of Sciences of the United States of America*, 118, <https://doi.org/10.1073/pnas.2026111118>, 2021.
- 881 Driscoll, C. T., Mason, R. P., Chan, H. M., Jacob, D. J., and Pirrone, N.: Mercury as a global pollutant: Sources, pathways, and
882 effects, *Environmental Science and Technology*, 47, 4967–4983, <https://doi.org/10.1021/es305071v>, 2013.
- 883 Durnford, D. and Dastoor, A.: The behavior of mercury in the cryosphere: A review of what we know from observations, *Journal
884 of Geophysical Research Atmospheres*, 116, <https://doi.org/10.1029/2010JD014809>, 2011.
- 885 Edwards, B. A., Kushner, D. S., Outridge, P. M., and Wang, F.: Fifty years of volcanic mercury emission research: Knowledge
886 gaps and future directions, *Science of the Total Environment*, 757, 143800, <https://doi.org/10.1016/j.scitotenv.2020.143800>,
887 2021.
- 888 Eftimi, R., Skende, P., and Zoto, J.: An isotope study of the connection of Ohrid and Prespa lakes, *Geologica Balcanica*, 32,
889 43–49, 1999.
- 890 Ehrmann, W. and Schmiedl, G.: Nature and dynamics of North African humid and dry periods during the last 200,000 years
891 documented in the clay fraction of eastern mediterranean deep-sea sediments, *Quaternary Science Reviews*, 260, 106925,
892 <https://doi.org/10.1016/j.quascirev.2021.106925>, 2021.
- 893 Engstrom, D. R. and Rose, N. L.: A whole-basin, mass-balance approach to paleolimnology, *J Paleolimnol*, 49, 333–347,
894 <https://doi.org/10.1007/s10933-012-9675-5>, 2013.
- 895 Engstrom, D. R. and Wright, H. E.: Chemical stratigraphy of lake sediments as a record of environmental change, in: *Lake
896 Sediments and Environmental History*, University of Minnesota Press, 11–67, 1984.
- 897 Fadina, O. A., Venancio, I. M., Belem, A., Silveira, C. S., Bertagnolli, D. de C., Silva-Filho, E. V., and Albuquerque, A. L. S.:
898 Paleoclimatic controls on mercury deposition in northeast Brazil since the Last Interglacial, *Quaternary Science Reviews*, 221,
899 105869, <https://doi.org/10.1016/j.quascirev.2019.105869>, 2019.
- 900 Figueiredo, T. S., Santos, T. P., Costa, K. B., Toledo, F., Albuquerque, A. L. S., Smoak, J. M., Bergquist, B. A., and Silva-Filho,
901 E. V.: Effect of deep Southwestern Subtropical Atlantic Ocean circulation on the biogeochemistry of mercury during the last two
902 glacial/interglacial cycles, *Quaternary Science Reviews*, 239, 106368, <https://doi.org/10.1016/j.quascirev.2020.106368>, 2020.
- 903 Figueiredo, T. S., Bergquist, B. A., Santos, T. P., Albuquerque, A. L. S., and Silva-Filho, E. V.: Relationship between glacial
904 CO₂ drawdown and mercury cycling in the western South Atlantic: An isotopic insight, *Geology*, 50, 3–7,
905 <https://doi.org/10.1130/g49942.1>, 2022.
- 906 Fitzgerald, W. F. and Lamborg, C. H.: *Geochemistry of Mercury in the Environment*, Elsevier Ltd., 91–129 pp.,
907 <https://doi.org/10.1016/B978-0-08-095975-7.00904-9>, 2013.
- 908 Fitzgerald, W. F., Engstrom, D. R., Lamborg, C. H., Tseng, C.-M., Balcom, P. H., and Hammerschmidt, C. R.: Modern and
909 Historic Atmospheric Mercury Fluxes in Northern Alaska: Global Sources and Arctic Depletion, *Environ. Sci. Technol.*, 39, 557–
910 568, <https://doi.org/10.1021/es049128x>, 2005.
- 911 Francke, A., Wagner, B., Just, J., Leicher, N., Gromig, R., Baumgarten, H., Vogel, H., Lacey, J. H., Sadori, L., Wonik, T., Leng,
912 M. J., Zanchetta, G., Sulpizio, R., and Giaccio, B.: Sedimentological processes and environmental variability at Lake Ohrid
913 (Macedonia, Albania) between 637 ka and the present, *Biogeosciences*, 13, 1179–1196, [https://doi.org/10.5194/bg-13-1179-
914 2016](https://doi.org/10.5194/bg-13-1179-2016), 2016.
- 915 Francke, A., Dosseto, A., Panagiotopoulos, K., Leicher, N., Lacey, J. H., Kyrikou, S., Wagner, B., Zanchetta, G., Kouli, K., and
916 Leng, M. J.: Sediment residence time reveals Holocene shift from climatic to vegetation control on catchment erosion in the
917 Balkans, *Global and Planetary Change*, 177, 186–200, <https://doi.org/10.1016/j.gloplacha.2019.04.005>, 2019.

- 918 Frieling, J., Mather, T. A., März, C., Jenkyns, H. C., Hennekam, R., Reichart, G.-J., Slomp, C. P., and Van Helmond, N. A. G.
 919 M.: Effects of redox variability and early diagenesis on marine sedimentary Hg records, *Geochimica et Cosmochimica Acta*,
 920 S0016703723001850, <https://doi.org/10.1016/j.gca.2023.04.015>, 2023.
- 921 Gajić-Kvašček, M., Stojanović, M. M., Šmit, Ž., Kantarelou, V., Karydas, A. G., Šljivar, D., Milovanović, D., and Andrić, V.: New
 922 evidence for the use of cinnabar as a colouring pigment in the Vinča culture, *Journal of Archaeological Science*, 39, 1025–
 923 1033, <https://doi.org/10.1016/j.jas.2011.11.023>, 2012.
- 924 Garcia-Ordiales, E., Covelli, S., Rico, J. M., Roqueñí, N., Fontolan, G., Flor-Blanco, G., Cienfuegos, P., and Loredo, J.:
 925 Occurrence and speciation of arsenic and mercury in estuarine sediments affected by mining activities (Asturias, northern
 926 Spain), *Chemosphere*, 198, 281–289, <https://doi.org/10.1016/j.chemosphere.2018.01.146>, 2018.
- 927 Gelety, V. F., Kalmykov, G. V., and Parkhomenko, I. Y.: Mercury in the sedimentary deposits of Lake Baikal, *Geochemistry
 928 International*, 45, 170–177, <https://doi.org/10.1134/S001670290702005X>, 2007.
- 929 Giaccio, B., Hajdas, I., Isaia, R., Deino, A., and Nomade, S.: High-precision ¹⁴C and ⁴⁰Ar/³⁹Ar dating of the Campanian
 930 Ignimbrite (Y-5) reconciles the time-scales of climatic-cultural processes at 40 ka, *Scientific Reports*, 7, 1–10,
 931 <https://doi.org/10.1038/srep45940>, 2017.
- 932 Goosse, H., Brovkin, V., Fichefet, T., Haarsma, R., Huybrechts, P., Jongma, J., Mouchet, A., Selten, F., Barriat, P. Y., Campin,
 933 J. M., Deleersnijder, E., Driesschaert, E., Goelzer, H., Janssens, I., Loutre, M. F., Morales Maqueda, M. A., Opsteegh, T.,
 934 Mathieu, P. P., Munhoven, G., Pettersson, E. J., Renssen, H., Roche, D. M., Schaeffer, M., Tartinville, B., Timmermann, A.,
 935 and Weber, S. L.: Description of the Earth system model of intermediate complexity LOVECLIM version 1.2, *Geoscientific
 936 Model Development*, 3, 603–633, <https://doi.org/10.5194/gmd-3-603-2010>, 2010.
- 937 Grasby, S. E., Them, T. R., Chen, Z., Yin, R., and Ardakani, O. H.: Mercury as a proxy for volcanic emissions in the geologic
 938 record, *Earth-Science Reviews*, 196, 102880, <https://doi.org/10.1016/j.earscirev.2019.102880>, 2019.
- 939 Gromig, R., Mechernich, S., Ribolini, A., Wagner, B., Zanchetta, G., Isola, I., Bini, M., and Dunai, T. J.: Evidence for a Younger
 940 Dryas deglaciation in the Galicica Mountains (FYROM) from cosmogenic ³⁶Cl, *Quaternary International*, 464, 352–363,
 941 <https://doi.org/10.1016/j.quaint.2017.07.013>, 2018.
- 942 Grygar, T. M., Mach, K., and Martinez, M.: Checklist for the use of potassium concentrations in siliciclastic sediments as
 943 paleoenvironmental archives, *Sedimentary Geology*, 382, 75–84, <https://doi.org/10.1016/j.sedgeo.2019.01.010>, 2019.
- 944 Guédron, S., Tolu, J., Brisset, E., Sabatier, P., Perrot, V., Bouchet, S., Develle, A. L., Bindler, R., Cossa, D., Fritz, S. C., and
 945 Baker, P. A.: Late Holocene volcanic and anthropogenic mercury deposition in the western Central Andes (Lake Chungará
 946 Chile), *Science of the Total Environment*, 662, 903–914, <https://doi.org/10.1016/j.scitotenv.2019.01.294>, 2019.
- 947 Han, S., Obraztsova, A., Pretto, P., Deheyn, D. D., Gieskes, J., and Tebo, B. M.: Sulfide and iron control on mercury speciation
 948 in anoxic estuarine sediment slurries, *Marine Chemistry*, 111, 214–220, <https://doi.org/10.1016/j.marchem.2008.05.002>, 2008.
- 949 Hermanns, Y. M., Cortizas, A. M., Arz, H., Stein, R., and Biester, H.: Untangling the influence of in-lake productivity and
 950 terrestrial organic matter flux on 4,250 years of mercury accumulation in Lake Hambre, Southern Chile, *Journal of
 951 Paleolimnology*, 49, 563–573, <https://doi.org/10.1007/s10933-012-9657-7>, 2013.
- 952 Hoffmann, N., Reicherter, K., Fernández-Steeger, T., and Grützner, C.: Evolution of ancient Lake Ohrid: a tectonic perspective,
 953 *Biogeosciences*, 7, 3377–3386, <https://doi.org/10.5194/bg-7-3377-2010>, 2010.
- 954 Hollis, G. E. and Stevenson, A. C.: The physical basis of the Lake Mikri Prespa systems: Geology, climate, hydrology and water
 955 quality, *Hydrobiologia*, 351, 1–19, <https://doi.org/10.1023/A:1003067115862>, 1997.
- 956 Holmer, M. and Storkholm, P.: Sulphate reduction and sulphur cycling in lake sediments: a review: Sulphate cycling in lake
 957 sediments, *Freshwater Biology*, 46, 431–451, <https://doi.org/10.1046/j.1365-2427.2001.00687.x>, 2001.
- 958 Howard, D., Macsween, K., Edwards, G. C., Desservettaz, M., Guérette, E. A., Paton-Walsh, C., Surawski, N. C., Sullivan, A.
 959 L., Weston, C., Volkova, L., Powell, J., Keywood, M. D., Reisen, F., and (Mick) Meyer, C. P.: Investigation of mercury emissions
 960 from burning of Australian eucalypt forest surface fuels using a combustion wind tunnel and field observations, *Atmospheric
 961 Environment*, 202, 17–27, <https://doi.org/10.1016/j.atmosenv.2018.12.015>, 2019.
- 962 Hughes, P. D. and Woodward, J. C.: Quaternary glaciation in the Mediterranean mountains: A new synthesis, *Geological
 963 Society Special Publication*, 433, 1–23, <https://doi.org/10.1144/SP433.14>, 2017.
- 964 Hughes, P. D., Woodward, J. C., Gibbard, P. L., Macklin, M. G., Gilmour, M. A., and Smith, G. R.: The glacial history of the
 965 Pindus Mountains, Greece, *Journal of Geology*, 114, 413–434, <https://doi.org/10.1086/504177>, 2006.
- 966 Hughes, P. D., Allard, J. L., and Woodward, J. C.: The Balkans: glacial landforms prior to the Last Glacial Maximum, *European
 967 Glacial Landscapes*, 323–332, <https://doi.org/10.1016/b978-0-12-823498-3.00034-0>, 2022.

- 968 Hughes, P. D., Allard, J. L., Woodward, J. C., and Pope, R. J. J.: The Balkans: glacial landforms during deglaciation, in:
969 European Glacial Landscapes, Elsevier, 221–231, <https://doi.org/10.1016/B978-0-323-91899-2.00055-3>, 2023.
- 970 Jiskra, M., Guédron, S., Tolu, J., Fritz, S. C., Baker, P. A., and Sonke, J. E.: Climatic Controls on a Holocene Mercury Stable
971 Isotope Sediment Record of Lake Titicaca, ACS Earth and Space Chemistry, 6, 346–357,
972 <https://doi.org/10.1021/acsearthspacechem.1c00304>, 2022.
- 973 Jitaru, P., Gabrielli, P., Marteel, A., Plane, J. M. C., Planchon, F. A. M., Gauchard, P. A., Ferrari, C. P., Boutron, C. F., Adams,
974 F. C., Hong, S., Cescon, P., and Barbante, C.: Atmospheric depletion of mercury over Antarctica during glacial periods, Nature
975 Geoscience, 2, 505–508, <https://doi.org/10.1038/ngeo549>, 2009.
- 976 Jovanovska, E., Cvetkoska, A., Hauffe, T., Levkov, Z., Wagner, B., Sulpizio, R., Francke, A., Albrecht, C., and Wilke, T.:
977 Differential resilience of ancient sister lakes Ohrid and Prespa to environmental disturbances during the Late Pleistocene,
978 Biogeosciences, 13, 1149–1161, <https://doi.org/10.5194/bg-13-1149-2016>, 2016.
- 979 Just, J., Nowaczyk, N., Francke, A., Sagnotti, L., and Wagner, B.: Climatic control on the occurrence of high-coercivity magnetic
980 minerals and preservation of greigite in a 640 ka sediment sequence from Lake Ohrid (Balkans), Biogeosciences Discussions,
981 12, 14215–14243, <https://doi.org/10.5194/bgd-12-14215-2015>, 2015.
- 982 Kita, I., Yamashita, T., Chiyonobu, S., Hasegawa, H., Sato, T., and Kuwahara, Y.: Mercury content in Atlantic sediments as a
983 new indicator of the enlargement and reduction of Northern Hemisphere ice sheets, Journal of Quaternary Science, 31, 167–
984 177, <https://doi.org/10.1002/jqs.2854>, 2016.
- 985 Kohler, S. G., Petrova, M. V., Digernes, M. G., Sanchez, N., Dufour, A., Simić, A., Ndungu, K., and Ardelan, M. V.: Arctic
986 Ocean's wintertime mercury concentrations limited by seasonal loss on the shelf, Nature Geoscience,
987 <https://doi.org/10.1038/s41561-022-00986-3>, 2022.
- 988 Kongchum, M., Hudnall, W. H., and Delaune, R. D.: Relationship between sediment clay minerals and total mercury, Journal of
989 Environmental Science and Health - Part A Toxic/Hazardous Substances and Environmental Engineering, 46, 534–539,
990 <https://doi.org/10.1080/10934529.2011.551745>, 2011.
- 991 Krstić, S., Zdravski, N., and Blinkova, M.: Implementing the WFD in River Basin Management Plans – A Case Study of Prespa
992 Lake Watershed, in: BALWOIS, 2012.
- 993 Kurz, A. Y., Blum, J. D., Washburn, S. J., and Baskaran, M.: Changes in the mercury isotopic composition of sediments from a
994 remote alpine lake in Wyoming, USA, Science of the Total Environment, 669, 973–982,
995 <https://doi.org/10.1016/j.scitotenv.2019.03.165>, 2019.
- 996 de Lacerda, L. D., Turcq, B., Sifeddine, A., and Cordeiro, R. C.: Mercury accumulation rates in Caço Lake, NE Brazil during the
997 past 20.000 years, Journal of South American Earth Sciences, 77, 42–50, <https://doi.org/10.1016/j.jsames.2017.04.008>, 2017.
- 998 Lacey, J. H. and Jones, M. D.: Quantitative reconstruction of early Holocene and last glacial climate on the Balkan Peninsula
999 using coupled hydrological and isotope mass balance modelling, Quaternary Science Reviews, 202, 109–121,
1000 <https://doi.org/10.1016/j.quascirev.2018.09.007>, 2018.
- 1001 Lacey, J. H., Leng, M. J., Francke, A., Sloane, H. H., Milodowski, A., Vogel, H., Baumgarten, H., Zanchetta, G., and Wagner,
1002 B.: Northern Mediterranean climate since the Middle Pleistocene: A 637 ka stable isotope record from Lake Ohrid
1003 (Albania/Macedonia), Biogeosciences, 13, 1801–1820, <https://doi.org/10.5194/bg-13-1801-2016>, 2016.
- 1004 Leicher, N., Giaccio, B., Zanchetta, G., Sulpizio, R., Albert, P. G., Tomlinson, E. L., Lagos, M., Francke, A., and Wagner, B.:
1005 Lake Ohrid's teprochronological dataset reveals 1.36 Ma of Mediterranean explosive volcanic activity, Scientific Data, 8, 1–14,
1006 <https://doi.org/10.1038/s41597-021-01013-7>, 2021.
- 1007 Leng, M. J., Baneschi, I., Zanchetta, G., Jex, C. N., Wagner, B., and Vogel, H.: Late Quaternary palaeoenvironmental
1008 reconstruction from Lakes Ohrid and Prespa (Macedonia/Albania border) using stable isotopes, Biogeosciences, 7, 3109–3122,
1009 <https://doi.org/10.5194/bg-7-3109-2010>, 2010.
- 1010 Leng, M. J., Wagner, B., Boehm, A., Panagiotopoulos, K., Vane, C. H., Snelling, A., Haidon, C., Woodley, E., Vogel, H.,
1011 Zanchetta, G., and Baneschi, I.: Understanding past climatic and hydrological variability in the mediterranean from Lake Prespa
1012 sediment isotope and geochemical record over the last glacial cycle, Quaternary Science Reviews, 66, 123–136,
1013 <https://doi.org/10.1016/j.quascirev.2012.07.015>, 2013.
- 1014 Leontaritis, A. D., Kouli, K., and Pavlopoulos, K.: The glacial history of Greece: a comprehensive review, Mediterranean
1015 Geoscience Reviews, 2, 65–90, <https://doi.org/10.1007/s42990-020-00021-w>, 2020.
- 1016 Lewin, J., Macklin, M. G., and Woodward, J. C.: Late quaternary fluvial sedimentation in the voidomatis basin, Epirus,
1017 Northwest Greece, Quaternary Research, 35, 103–115, [https://doi.org/10.1016/0033-5894\(91\)90098-P](https://doi.org/10.1016/0033-5894(91)90098-P), 1991.
- 1018 Lézine, A. M., von Grafenstein, U., Andersen, N., Belmecheri, S., Bordon, A., Caron, B., Cazet, J. P., Erlenkeuser, H.,
1019 Fouache, E., Grenier, C., Huntsman-Mapila, P., Hureau-Mazaudier, D., Manelli, D., Mazaud, A., Robert, C., Sulpizio, R.,

- 1020 Tiercelin, J. J., Zanchetta, G., and Zeqollari, Z.: Lake Ohrid, Albania, provides an exceptional multi-proxy record of
 1021 environmental changes during the last glacial-interglacial cycle, *Palaeogeography, Palaeoclimatology, Palaeoecology*, 287,
 1022 116–127, <https://doi.org/10.1016/j.palaeo.2010.01.016>, 2010.
- 1023 Li, C., Enrico, M., Magand, O., Araujo, B. F., Le Roux, G., Osterwalder, S., Dommergue, A., Bertrand, Y., Brioude, J., De
 1024 Vleeschouwer, F., and Sonke, J. E.: A peat core Hg stable isotope reconstruction of Holocene atmospheric Hg deposition at
 1025 Amsterdam Island (37.8oS), *Geochimica et Cosmochimica Acta*, 341, 62–74, <https://doi.org/10.1016/j.gca.2022.11.024>, 2023.
- 1026 Li, F., Ma, C., and Zhang, P.: Mercury Deposition, Climate Change and Anthropogenic Activities: A Review, *Frontiers in Earth
 1027 Science*, 8, <https://doi.org/10.3389/feart.2020.00316>, 2020.
- 1028 Lindhorst, K., Krastel, S., Reicherter, K., Stipp, M., Wagner, B., and Schwenk, T.: Sedimentary and tectonic evolution of Lake
 1029 Ohrid (Macedonia/Albania), *Basin Res.*, 27, 84–101, <https://doi.org/10.1111/bre.12063>, 2015.
- 1030 Lisiecki, L. E. and Raymo, M. E.: A Pliocene-Pleistocene stack of 57 globally distributed benthic δ 18O records,
 1031 *Paleoceanography*, 20, 1–17, <https://doi.org/10.1029/2004PA001071>, 2005.
- 1032 Longman, J., Veres, D., Finsinger, W., and Ersek, V.: Exceptionally high levels of lead pollution in the Balkans from the Early
 1033 Bronze Age to the Industrial Revolution, *Proc. Natl. Acad. Sci. U.S.A.*, 115, <https://doi.org/10.1073/pnas.1721546115>, 2018.
- 1034 Lyman, S. N., Cheng, I., Gratz, L. E., Weiss-Penzias, P., and Zhang, L.: An updated review of atmospheric mercury, *Science of
 1035 the Total Environment*, 707, 135575, <https://doi.org/10.1016/j.scitotenv.2019.135575>, 2020.
- 1036 Masi, A., Francke, A., Pepe, C., Thienemann, M., Wagner, B., and Sadori, L.: Vegetation history and paleoclimate at Lake
 1037 Dojran (FYROM/Greece) during the Late Glacial and Holocene, *Clim. Past*, 14, 351–367, <https://doi.org/10.5194/cp-14-351-2018>, 2018.
- 1039 Mataix-Solera, J., Cerdà, A., Arcenegui, V., Jordán, A., and Zavala, L. M.: Fire effects on soil aggregation: A review, *Earth-
 1040 Science Reviews*, 109, 44–60, <https://doi.org/10.1016/j.earscirev.2011.08.002>, 2011.
- 1041 Matzinger, A., Jordanoski, M., Veljanoska-Sarafiloska, E., Sturm, M., Müller, B., and Wüest, A.: Is Lake Prespa jeopardizing the
 1042 ecosystem of ancient Lake Ohrid?, *Hydrobiologia*, 553, 89–109, <https://doi.org/10.1007/s10750-005-6427-9>, 2006.
- 1043 Melendez-Perez, J. J., Fostier, A. H., Carvalho, J. A., Windmöller, C. C., Santos, J. C., and Carpi, A.: Soil and biomass mercury
 1044 emissions during a prescribed fire in the Amazonian rain forest, *Atmospheric Environment*, 96, 415–422,
 1045 <https://doi.org/10.1016/j.atmosenv.2014.06.032>, 2014.
- 1046 Nasr, M., Ogilvie, J., Castonguay, M., Rencz, A., and Arp, P. A.: Total Hg concentrations in stream and lake sediments:
 1047 Discerning geospatial patterns and controls across Canada, *Applied Geochemistry*, 26, 1818–1831,
 1048 <https://doi.org/10.1016/j.apgeochem.2011.06.006>, 2011.
- 1049 Obrist, D., Kirk, J. L., Zhang, L., Sunderland, E. M., Jiskra, M., and Selin, N. E.: A review of global environmental mercury
 1050 processes in response to human and natural perturbations: Changes of emissions, climate, and land use, *Ambio*, 47, 116–140,
 1051 <https://doi.org/10.1007/s13280-017-1004-9>, 2018.
- 1052 Oliva, M., Žebre, M., Guglielmin, M., Hughes, P. D., Çiner, A., Vieira, G., Bodin, X., Andrés, N., Colucci, R. R., García-
 1053 Hernández, C., Mora, C., Nofre, J., Palacios, D., Pérez-Alberti, A., Ribolini, A., Ruiz-Fernández, J., Sarıkaya, M. A., Serrano,
 1054 E., Urdea, P., Valcárcel, M., Woodward, J. C., and Yıldırım, C.: Permafrost conditions in the Mediterranean region since the
 1055 Last Glaciation, *Earth-Science Reviews*, 185, 397–436, <https://doi.org/10.1016/j.earscirev.2018.06.018>, 2018.
- 1056 Outridge, Sanei, H., Stern, Hamilton, and Goodarzi, F.: Evidence for Control of Mercury Accumulation Rates in Canadian High
 1057 Arctic Lake Sediments by Variations of Aquatic Primary Productivity, *Environ. Sci. Technol.*, 41, 5259–5265,
 1058 <https://doi.org/10.1021/es070408x>, 2007.
- 1059 Outridge, P. M., Mason, R. P., Wang, F., Guerrero, S., and Heimbürger-Boavida, L. E.: Updated Global and Oceanic Mercury
 1060 Budgets for the United Nations Global Mercury Assessment 2018, *Environmental Science and Technology*, 52, 11466–11477,
 1061 <https://doi.org/10.1021/acs.est.8b01246>, 2018.
- 1062 Outridge, P. M., Stern, G. A., Hamilton, P. B., and Sanei, H.: Algal scavenging of mercury in preindustrial Arctic lakes, *Limnol
 1063 Oceanogr.*, 64, 1558–1571, <https://doi.org/10.1002/lno.11135>, 2019.
- 1064 Overeem, I., Hudson, B. D., Syvitski, J. P. M., Mikkelsen, A. B., Hasholt, B., Van Den Broeke, M. R., Noel, B. P. Y., and
 1065 Morlighem, M.: Substantial export of suspended sediment to the global oceans from glacial erosion in Greenland, *Nature
 1066 Geoscience*, 10, 859–863, <https://doi.org/10.1038/NGEO3046>, 2017.
- 1067 Pan, J., Zhong, W., Wei, Z., Ouyang, J., Shang, S., Ye, S., Chen, Y., Xue, J., and Tang, X.: A 15,400-year record of natural and
 1068 anthropogenic input of mercury (Hg) in a sub-alpine lacustrine sediment succession from the western Nanling Mountains, South
 1069 China, *Environmental Science and Pollution Research*, 27, 20478–20489, <https://doi.org/10.1007/s11356-020-08421-z>, 2020.

- 1070 Panagiotopoulos, K.: Late Quaternary ecosystem and climate interactions in SW Balkans inferred from Lake Prespa sediments, Universität zu Köln, Cologne, Germany, 2013.
1071
- 1072 Panagiotopoulos, K., Aufgebauer, A., Schäbitz, F., and Wagner, B.: Vegetation and climate history of the Lake Prespa region since the Lateglacial, *Quaternary International*, 293, 157–169, <https://doi.org/10.1016/j.quaint.2012.05.048>, 2013.
1073
- 1074 Panagiotopoulos, K., Böhm, A., Leng, M. J., Wagner, B., and Schäbitz, F.: Climate variability over the last 92 ka in SW Balkans from analysis of sediments from Lake Prespa, *Climate of the Past*, 10, 643–660, <https://doi.org/10.5194/cp-10-643-2014>, 2014.
1075
- 1076 Panagiotopoulos, K., Holtvoeth, J., Kouli, K., Marinova, E., Francke, A., Cvetkoska, A., Jovanovska, E., Lacey, J. H., Lyons, E. T., Buckel, C., Bertini, A., Donders, T., Just, J., Leicher, N., Leng, M. J., Melles, M., Pancost, R. D., Sadori, L., Tauber, P., Vogel, H., Wagner, B., and Wilke, T.: Insights into the evolution of the young Lake Ohrid ecosystem and vegetation succession from a southern European refugium during the Early Pleistocene, *Quaternary Science Reviews*, 227, <https://doi.org/10.1016/j.quascirev.2019.106044>, 2020.
1077
1078
1079
1080
- 1081 Percival, L. M. E., Witt, M. L. I., Mather, T. A., Hermoso, M., Jenkyns, H. C., Hesselbo, S. P., Al-Suwaidi, A. H., Storm, M. S., Xu, W., and Ruhl, M.: Globally enhanced mercury deposition during the end-Pliensbachian extinction and Toarcian OAE: A link to the Karoo-Ferrar Large Igneous Province, *Earth and Planetary Science Letters*, 428, 267–280, <https://doi.org/10.1016/j.epsl.2015.06.064>, 2015.
1082
1083
1084
- 1085 Percival, L. M. E., Jenkyns, H. C., Mather, T. A., Dickson, A. J., Batenburg, S. J., Ruhl, M., Hesselbo, S. P., Barclay, R., Jarvis, I., Robinson, S. A., and Woelders, L.: Does large igneous province volcanism always perturb the mercury cycle? Comparing the records of Oceanic Anoxic Event 2 and the end-cretaceous to other Mesozoic events, *American Journal of Science*, 318, 799–860, <https://doi.org/10.2475/08.2018.01>, 2018.
1086
1087
1088
- 1089 Pérez-Rodríguez, M., Horák-Terra, I., Rodríguez-Lado, L., Aboal, J. R., and Martínez Cortizas, A.: Long-Term (~57 ka) controls on mercury accumulation in the southern hemisphere reconstructed using a peat record from pinheiro mire (minas gerais, Brazil), *Environmental Science and Technology*, 49, 1356–1364, <https://doi.org/10.1021/es504826d>, 2015.
1090
1091
- 1092 Pérez-Rodríguez, M., Margalef, O., Corella, J. P., Saiz-Lopez, A., Pla-Rabes, S., Giralt, S., and Cortizas, A. M.: The role of climate: 71 ka of atmospheric mercury deposition in the southern hemisphere recorded by Rano Aroi Mire, Easter Island (Chile), *Geosciences (Switzerland)*, 8, <https://doi.org/10.3390/geosciences8100374>, 2018.
1093
1094
- 1095 Pope, R. J., Hughes, P. D., and Skourtsos, E.: Glacial history of Mt Chelmos, Peloponnesus, Greece, *Geological Society Special Publication*, 433, 211–236, <https://doi.org/10.1144/SP433.11>, 2017.
1096
- 1097 Radivojević, M. and Roberts, B. W.: Early Balkan Metallurgy: Origins, Evolution and Society, 6200–3700 BC, Springer US, 195–278 pp., <https://doi.org/10.1007/s10963-021-09155-7>, 2021.
1098
- 1099 Rasmussen, S. O., Bigler, M., Blockley, S. P., Blunier, T., Buchardt, S. L., Clausen, H. B., Cvijanovic, I., Dahl-Jensen, D., Johnsen, S. J., Fischer, H., Gkinis, V., Guillevic, M., Hoek, W. Z., Lowe, J. J., Pedro, J. B., Popp, T., Seierstad, I. K., Steffensen, J. P., Svensson, A. M., Vallelonga, P., Vinther, B. M., Walker, M. J. C., Wheatley, J. J., and Winstrup, M.: A stratigraphic framework for abrupt climatic changes during the Last Glacial period based on three synchronized Greenland ice-core records: Refining and extending the INTIMATE event stratigraphy, *Quaternary Science Reviews*, 106, 14–28, <https://doi.org/10.1016/j.quascirev.2014.09.007>, 2014.
1100
1101
1102
1103
1104
- 1105 Ravichandran, M.: Interactions between mercury and dissolved organic matter - A review, *Chemosphere*, 55, 319–331, <https://doi.org/10.1016/j.chemosphere.2003.11.011>, 2004.
1106
- 1107 Reimer, P. J., Austin, W. E. N., Bard, E., Bayliss, A., Blackwell, P. G., Bronk Ramsey, C., Butzin, M., Cheng, H., Edwards, R. L., Friedrich, M., Grootes, P. M., Guilderson, T. P., Hajdas, I., Heaton, T. J., Hogg, A. G., Hughen, K. A., Kromer, B., Manning, S. W., Muscheler, R., Palmer, J. G., Pearson, C., Van Der Plicht, J., Reimer, R. W., Richards, D. A., Scott, E. M., Southon, J. R., Turney, C. S. M., Wacker, L., Adolphi, F., Büntgen, U., Capano, M., Fahrni, S. M., Fogtmann-Schulz, A., Friedrich, R., Köhler, P., Kudsk, S., Miyake, F., Olsen, J., Reinig, F., Sakamoto, M., Sookdeo, A., and Talamo, S.: The IntCal20 Northern Hemisphere Radiocarbon Age Calibration Curve (0-55 cal kBP), *Radiocarbon*, 62, 725–757, <https://doi.org/10.1017/RDC.2020.41>, 2020.
1108
1109
1110
1111
1112
1113
- 1114 Ribolini, A., Isola, I., Zanchetta, G., Bini, M., and Sulpizio, R.: Glacial features on the Galicica Mountains, Macedonia: Preliminary report, *Geografia Fisica e Dinamica Quaternaria*, 34, 247–255, <https://doi.org/10.4461/GFDQ.2011.34.22>, 2011.
1115
- 1116 Ribolini, A., Bini, M., Isola, I., Spagnolo, M., Zanchetta, G., Pellitero, R., Mechernich, S., Gromig, R., Dunai, T., Wagner, B., and Milevski, I.: An oldest dryas glacier expansion on mount pelister (former Yugoslavian Republic of Macedonia) according to ¹⁰Be cosmogenic dating, *Journal of the Geological Society*, 175, 100–110, <https://doi.org/10.1144/jgs2017-038>, 2018.
1117
1118
- 1119 Roshan, A. and Biswas, A.: Fire-induced geochemical changes in soil: Implication for the element cycling, *Science of The Total Environment*, 868, 161714, <https://doi.org/10.1016/j.scitotenv.2023.161714>, 2023.
1120
- 1121 Rothacker, L., Dosseto, A., Francke, A., Chivas, A. R., Vigier, N., Kotarba-Morley, A. M., and Menozzi, D.: Impact of climate change and human activity on soil landscapes over the past 12,300 years, *Sci Rep*, 8, 247, <https://doi.org/10.1038/s41598-017-18603-4>, 2018.
1122
1123

- 1124 Rousseau, D.-D., Antoine, P., and Sun, Y.: How dusty was the last glacial maximum over Europe?, *Quaternary Science*
1125 *Reviews*, 254, 106775, <https://doi.org/10.1016/j.quascirev.2020.106775>, 2021.
- 1126 Ruszkiczay-Rüdiger, Z., Kern, Z., Temovski, M., Madarász, B., Milevski, I., and Braucher, R.: Last deglaciation in the central
1127 Balkan Peninsula: Geochronological evidence from the Jablanica Mt. (North Macedonia), *Geomorphology*, 351,
1128 <https://doi.org/10.1016/j.geomorph.2019.106985>, 2020.
- 1129 Rytuba, J. J.: Mercury from mineral deposits and potential environmental impact, *Environmental Geology*, 43, 326–338,
1130 <https://doi.org/10.1007/s00254-002-0629-5>, 2003.
- 1131 Sadori, L., Koutsodendris, A., Panagiotopoulos, K., Masi, A., Bertini, A., Combourieu-Nebout, N., Francke, A., Kouli, K., Kousis,
1132 I., Joannin, S., Maria Mercuri, A., Peyron, O., Torri, P., Wagner, B., Zanchetta, G., Sinopoli, G., and Donders, T. H.:
1133 Corrigendum to “Pollen-based paleoenvironmental and paleoclimatic change at Lake Ohrid (south-eastern Europe) during the
1134 past 500 ka,” *Biogeosciences*, 13, 1423–1427, <https://doi.org/10.5194/bg-13-1423-2016-corrigendum>, 2016a.
- 1135 Sadori, L., Koutsodendris, A., Panagiotopoulos, K., Masi, A., Bertini, A., Combourieu-Nebout, N., Francke, A., Kouli, K.,
1136 Joannin, S., Mercuri, A. M., Peyron, O., Torri, P., Wagner, B., Zanchetta, G., Sinopoli, G., and Donders, T. H.: Pollen-based
1137 paleoenvironmental and paleoclimatic change at Lake Ohrid (south-eastern Europe) during the past 500 ka, *Biogeosciences*,
1138 13, 1423–1437, <https://doi.org/10.5194/bg-13-1423-2016>, 2016b.
- 1139 Sanchez Goñi, M. F. and Harrison, S. P.: Millennial-scale climate variability and vegetation changes during the Last Glacial:
1140 Concepts and terminology, *Quaternary Science Reviews*, 29, 2823–2827, <https://doi.org/10.1016/j.quascirev.2009.11.014>,
1141 2010.
- 1142 Sanei, H., Grasby, S., and Beauchamp, B.: Latest Permian mercury anomalies, *Geology*, 40, 63–66, 2012.
- 1143 Scaillet, S., Vita-Scaillet, G., and Rotolo, S. G.: Millennial-scale phase relationships between ice-core and Mediterranean
1144 marine records: Insights from high-precision $^{40}\text{Ar}/^{39}\text{Ar}$ dating of the Green Tuff of Pantelleria, Sicily Strait, *Quaternary Science*
1145 *Reviews*, 78, 141–154, <https://doi.org/10.1016/j.quascirev.2013.08.008>, 2013.
- 1146 Schlüter, K.: Review: Evaporation of mercury from soils. An integration and synthesis of current knowledge, *Environmental*
1147 *Geology*, 39, 249–271, <https://doi.org/10.1007/s002540050005>, 2000.
- 1148 Schneider, L., Cooke, C. A., Stansell, N. D., and Haberle, S. G.: Effects of climate variability on mercury deposition during the
1149 Older Dryas and Younger Dryas in the Venezuelan Andes, *Journal of Paleolimnology*, 63, 211–224,
1150 <https://doi.org/10.1007/s10933-020-00111-7>, 2020.
- 1151 Schotsmans, E. M. J., Busacca, G., Lin, S. C., Vasić, M., Lingle, A. M., Veropoulidou, R., Mazzucato, C., Tibbetts, B., Haddow,
1152 S. D., Somel, M., Toksoy-Köksal, F., Knüsel, C. J., and Milella, M.: New insights on commemoration of the dead through
1153 mortuary and architectural use of pigments at Neolithic Çatalhöyük, Turkey, *Sci Rep*, 12, 4055, <https://doi.org/10.1038/s41598-022-07284-3>, 2022.
- 1155 Schuster, P. F., Schaefer, K. M., Aiken, G. R., Antweiler, R. C., Dewild, J. F., Gryziec, J. D., Gusmeroli, A., Hugelius, G.,
1156 Jafarov, E., Krabbenhoft, D. P., Liu, L., Herman-Mercer, N., Mu, C., Roth, D. A., Schaefer, T., Striegl, R. G., Wickland, K. P.,
1157 and Zhang, T.: Permafrost Stores a Globally Significant Amount of Mercury, *Geophysical Research Letters*, 45, 1463–1471,
1158 <https://doi.org/10.1002/2017GL075571>, 2018.
- 1159 Schütze, M., Tserendorj, G., Pérez-Rodríguez, M., Rösch, M., and Biester, H.: Prediction of Holocene mercury accumulation
1160 trends by combining palynological and geochemical records of lake sediments (Black Forest, Germany), *Geosciences*
1161 (Switzerland), 8, <https://doi.org/10.3390/geosciences8100358>, 2018.
- 1162 Selin, N. E.: Global biogeochemical cycling of mercury: a review, *Annual Review of Environmental Resources*, 34, 43–63,
1163 2009.
- 1164 Shakesby, R. A.: Post-wildfire soil erosion in the Mediterranean: Review and future research directions, *Earth-Science*
1165 *Reviews*, 105, 71–100, <https://doi.org/10.1016/j.earscirev.2011.01.001>, 2011.
- 1166 Shen, J., Feng, Q., Algeo, T. J., Liu, J., Zhou, C., Wei, W., Liu, J., Them, T. R., Gill, B. C., and Chen, J.: Sedimentary host
1167 phases of mercury (Hg) and implications for use of Hg as a volcanic proxy, *Earth and Planetary Science Letters*, 543, 116333,
1168 <https://doi.org/10.1016/j.epsl.2020.116333>, 2020.
- 1169 Sial, A. N., Lacerda, L. D., Ferreira, V. P., Frei, R., Marquillas, R. A., Barbosa, J. A., Gaucher, C., Windmüller, C. C., and
1170 Pereira, N. S.: Mercury as a proxy for volcanic activity during extreme environmental turnover: The Cretaceous-Paleogene
1171 transition, *Palaeogeography, Palaeoclimatology, Palaeoecology*, 387, 153–164, <https://doi.org/10.1016/j.palaeo.2013.07.019>,
1172 2013.
- 1173 Simonsen, M. F., Baccolo, G., Blunier, T., Borunda, A., Delmonte, B., Frei, R., Goldstein, S., Grinsted, A., Kjær, H. A., Sowers,
1174 T., Svensson, A., Vinther, B., Vladimirova, D., Winckler, G., Winstrup, M., and Vallenga, P.: East Greenland ice core dust
1175 record reveals timing of Greenland ice sheet advance and retreat, *Nature Communications*, 10, <https://doi.org/10.1038/s41467-019-12546-2>, 2019.

- 1177 Soerensen, Anne. L., Schartup, A. T., Gustafsson, E., Gustafsson, B. G., Undeman, E., and Björn, E.: Eutrophication Increases
1178 Phytoplankton Methylmercury Concentrations in a Coastal Sea—A Baltic Sea Case Study, *Environ. Sci. Technol.*, 50, 11787–
1179 11796, <https://doi.org/10.1021/acs.est.6b02717>, 2016.
- 1180 Stern, G. A., Sanei, H., Roach, P., DeLaronde, J., and Outridge, P. M.: Historical Interrelated Variations of Mercury and Aquatic
1181 Organic Matter in Lake Sediment Cores from a Subarctic Lake in Yukon, Canada: Further Evidence toward the Algal-Mercury
1182 Scavenging Hypothesis, *Environ. Sci. Technol.*, 43, 7684–7690, <https://doi.org/10.1021/es902186s>, 2009.
- 1183 Streets, D. G., Horowitz, H. M., Lu, Z., Levin, L., Thackray, C. P., and Sunderland, E. M.: Five hundred years of anthropogenic
1184 mercury: spatial and temporal release profiles*, *Environ. Res. Lett.*, 14, 084004, <https://doi.org/10.1088/1748-9326/ab281f>,
1185 2019.
- 1186 Styllas, M. N., Schimmelpfennig, I., Benedetti, L., Ghilardi, M., Aumaitre, G., Bourlès, D., and Keddadouche, K.: Late-glacial
1187 and Holocene history of the northeast Mediterranean mountains - New insights from in situ-produced ³⁶Cl-based cosmic ray
1188 exposure dating of paleo-glacier deposits on Mount Olympus, Greece, *Quaternary Science Reviews*, 193, 244–265,
1189 <https://doi.org/10.1016/j.quascirev.2018.06.020>, 2018.
- 1190 Takenaka, C., Shibata, H., Tomiyasu, T., Yasumatsu, S., and Muraio, S.: Effects of forest fires on mercury accumulation in soil
1191 at the artisanal small-scale gold mining, *Environ Monit Assess*, 193, 699, <https://doi.org/10.1007/s10661-021-09394-3>, 2021.
- 1192 Them, T. R., Jagoe, C. H., Caruthers, A. H., Gill, B. C., Grasby, S. E., Gröcke, D. R., Yin, R., and Owens, J. D.: Terrestrial
1193 sources as the primary delivery mechanism of mercury to the oceans across the Toarcian Oceanic Anoxic Event (Early
1194 Jurassic), *Earth and Planetary Science Letters*, 507, 62–72, <https://doi.org/10.1016/j.epsl.2018.11.029>, 2019.
- 1195 Thienemann, M., Masi, A., Kusch, S., Sadori, L., John, S., Francke, A., Wagner, B., and Rethemeyer, J.: Organic geochemical
1196 and palynological evidence for Holocene natural and anthropogenic environmental change at Lake Dojran
1197 (Macedonia/Greece), *The Holocene*, 27, 1103–1114, <https://doi.org/10.1177/0959683616683261>, 2017.
- 1198 Tisserand, D., Guéron, S., Viollier, E., Jézéquel, D., Rigaud, S., Campillo, S., Sarret, G., Charlet, L., and Cossa, D.: Mercury,
1199 organic matter, iron, and sulfur co-cycling in a ferruginous meromictic lake, *Applied Geochemistry*, 146, 105463,
1200 <https://doi.org/10.1016/j.apgeochem.2022.105463>, 2022.
- 1201 Tzedakis, P. C., Hooghiemstra, H., and Pälike, H.: The last 1.35 million years at Tenaghi Philippon: revised chronostratigraphy
1202 and long-term vegetation trends, *Quaternary Science Reviews*, 25, 3416–3430,
1203 <https://doi.org/10.1016/j.quascirev.2006.09.002>, 2006.
- 1204 Újvári, G., Kovács, J., Varga, G., Raucsik, B., and Marković, S. B.: Dust flux estimates for the Last Glacial Period in East
1205 Central Europe based on terrestrial records of loess deposits: A review, *Quaternary Science Reviews*, 29, 3157–3166,
1206 <https://doi.org/10.1016/j.quascirev.2010.07.005>, 2010.
- 1207 Ulfers, A., Zeeden, C., Wagner, B., Krastel, S., Buness, H., and Wonik, T.: Borehole logging and seismic data from Lake Ohrid
1208 (North Macedonia/Albania) as a basis for age-depth modelling over the last one million years, *Quaternary Science Reviews*,
1209 276, 107295, <https://doi.org/10.1016/j.quascirev.2021.107295>, 2022.
- 1210 United Nations Environment Programme: Global Mercury Assessment, United Nations, 2018.
- 1211 Vandal, G. M., Fitzgerald, W. F., Boutron, C. F., and Candelone, J. P.: Variations in mercury deposition to Antarctica over the
1212 past 34,000 years, *Nature*, 362, 621–623, <https://doi.org/10.1038/362621a0>, 1993.
- 1213 Vogel, H., Wagner, B., Zanchetta, G., Sulpizio, R., and Rosén, P.: A paleoclimate record with tephrochronological age control
1214 for the last glacial-interglacial cycle from Lake Ohrid, Albania and Macedonia, *Journal of Paleolimnology*, 44, 295–310,
1215 <https://doi.org/10.1007/s10933-009-9404-x>, 2010.
- 1216 Wagner, B., Lotter, A. F., Nowaczyk, N., Reed, J. M., Schwalb, A., Sulpizio, R., Valsecchi, V., Wessels, M., and Zanchetta, G.:
1217 A 40,000-year record of environmental change from ancient Lake Ohrid (Albania and Macedonia), *Journal of Paleolimnology*,
1218 41, 407–430, <https://doi.org/10.1007/s10933-008-9234-2>, 2009.
- 1219 Wagner, B., Vogel, H., Zanchetta, G., and Sulpizio, R.: Environmental change within the Balkan region during the past ca. 50
1220 ka recorded in the sediments from lakes Prespa and Ohrid, *Biogeosciences*, 7, 3187–3198, [https://doi.org/10.5194/bg-7-3187-](https://doi.org/10.5194/bg-7-3187-2010)
1221 2010, 2010.
- 1222 Wagner, B., Aufgebauer, A., Vogel, H., Zanchetta, G., Sulpizio, R., and Damaschke, M.: Late Pleistocene and Holocene
1223 contourite drift in Lake Prespa (Albania/F.Y.R. of Macedonia/Greece), *Quaternary International*, 274, 112–121,
1224 <https://doi.org/10.1016/j.quaint.2012.02.016>, 2012.
- 1225 Wagner, B., Leng, M. J., Wilke, T., Böhm, A., Panagiotopoulos, K., Vogel, H., Lacey, J. H., Zanchetta, G., and Sulpizio, R.:
1226 Distinct lake level lowstand in Lake Prespa (SE Europe) at the time of the 74 (75) ka Toba eruption, *Climate of the Past*, 10,
1227 261–267, <https://doi.org/10.5194/cp-10-261-2014>, 2014a.

- 1228 Wagner, B., Wilke, T., Krastel, S., Zanchetta, G., Sulpizio, R., Reicherter, K., Leng, M. J., Grazhdani, A., Trajanovski, S.,
1229 Francke, A., Lindhorst, K., Levkov, Z., Cvetkoska, A., Reed, J. M., Zhang, X., Lacey, J. H., Wonik, T., Baumgarten, H., and
1230 Vogel, H.: The SCOPSCO drilling project recovers more than 1.2 million years of history from Lake Ohrid, *Sci. Dril.*, 17, 19–29,
1231 <https://doi.org/10.5194/sd-17-19-2014>, 2014b.
- 1232 Wagner, B., Vogel, H., Francke, A., Friedrich, T., Donders, T., Lacey, J. H., Leng, M. J., Regattieri, E., Sadori, L., Wilke, T.,
1233 Zanchetta, G., Albrecht, C., Bertini, A., Combourieu-Nebout, N., Cvetkoska, A., Giaccio, B., Grazhdani, A., Hauffe, T.,
1234 Holtvoeth, J., Joannin, S., Jovanovska, E., Just, J., Kouli, K., Kousis, I., Koutsodendris, A., Krastel, S., Lagos, M., Leicher, N.,
1235 Levkov, Z., Lindhorst, K., Masi, A., Melles, M., Mercuri, A. M., Nomade, S., Nowaczyk, N., Panagiotopoulos, K., Peyron, O.,
1236 Reed, J. M., Sagnotti, L., Sinopoli, G., Stelbrink, B., Sulpizio, R., Timmermann, A., Tofilovska, S., Torri, P., Wagner-Cremer, F.,
1237 Wonik, T., and Zhang, X.: Mediterranean winter rainfall in phase with African monsoons during the past 1.36 million years,
1238 *Nature*, 573, 256–260, <https://doi.org/10.1038/s41586-019-1529-0>, 2019.
- 1239 Wagner, B., Tauber, P., Francke, A., Leicher, N., Binnie, S. A., Cvetkoska, A., Jovanovska, E., Just, J., Lacey, J. H., Levkov, Z.,
1240 Lindhorst, K., Kouli, K., Krastel, S., Pana-giotopoulos, K., Ulfers, A., Zaova, D., Donders, T. H., Grazhdani, A., Koutsodendris,
1241 A., Leng, M. J., Sadori, L., Scheinert, M., Vogel, H., Wonik, T., Zanchetta, G., and Wilke, T.: The geodynamic and limnological
1242 evolution of Balkan Lake Ohrid, possibly the oldest extant lake in Europe, *Boreas*, bor.12601,
1243 <https://doi.org/10.1111/bor.12601>, 2022.
- 1244 Wang, F., Outridge, P. M., Feng, X., Meng, B., Heimbürger-Boavida, L. E., and Mason, R. P.: How closely do mercury trends in
1245 fish and other aquatic wildlife track those in the atmosphere? – Implications for evaluating the effectiveness of the Minamata
1246 Convention, *Science of the Total Environment*, 674, 58–70, <https://doi.org/10.1016/j.scitotenv.2019.04.101>, 2019.
- 1247 Warriar, A. K., Pednekar, H., Mahesh, B. S., Mohan, R., and Gazi, S.: Sediment grain size and surface textural observations of
1248 quartz grains in late quaternary lacustrine sediments from Schirmacher Oasis, East Antarctica: Paleoenvironmental
1249 significance, *Polar Science*, 10, 89–100, <https://doi.org/10.1016/j.polar.2015.12.005>, 2016.
- 1250 Watanabe, T., Naraoka, H., Nishimura, M., and Kawai, T.: Biological and environmental changes in Lake Baikal during the late
1251 Quaternary inferred from carbon, nitrogen and sulfur isotopes, *Earth and Planetary Science Letters*, 222, 285–299,
1252 <https://doi.org/10.1016/j.epsl.2004.02.009>, 2004.
- 1253 Woodward, J. C., Hamlin, R. H. B., Macklin, M. G., Hughes, P. D., and Lewin, J.: Glacial activity and catchment dynamics in
1254 northwest Greece: Long-term river behaviour and the slackwater sediment record for the last glacial to interglacial transition,
1255 *Geomorphology*, 101, 44–67, <https://doi.org/10.1016/j.geomorph.2008.05.018>, 2008.
- 1256 Zaferani, S. and Biester, H.: Mercury Accumulation in Marine Sediments – A Comparison of an Upwelling Area and Two Large
1257 River Mouths, *Front. Mar. Sci.*, 8, 732720, <https://doi.org/10.3389/fmars.2021.732720>, 2021.
- 1258 Zanchetta, G., Giaccio, B., Bini, M., and Sarti, L.: Tephrostratigraphy of Grotta del Cavallo, Southern Italy: Insights on the
1259 chronology of Middle to Upper Palaeolithic transition in the Mediterranean, *Quaternary Science Reviews*, 182, 65–77,
1260 <https://doi.org/10.1016/j.quascirev.2017.12.014>, 2018.
- 1261 Zhang, Q., Huang, J., Wang, F., Mark, L., Xu, J., Armstrong, D., Li, C., Zhang, Y., and Kang, S.: Mercury distribution and
1262 deposition in glacier snow over Western China, *Environmental Science and Technology*, 46, 5404–5413,
1263 <https://doi.org/10.1021/es300166x>, 2012.
- 1264